Plant Physiology Preview. Published on August 3, 2018, as DOI:10.1104/pp.18.00704

**Short title: $NO_2$ induces basal pathogen resistance**

**Corresponding author details:**
Dr. Frank Gaupels
Institute of Biochemical Plant Pathology, Helmholtz Zentrum München, German Research Center for Environmental Health, Ingolstädter Landstraße 1, 85764 Neuherberg, Germany
frank.gaupels@helmholtz-muenchen.de

**Research area:** Signaling and Response

# Short-term exposure to nitrogen dioxide provides basal pathogen resistance

Dörte Mayer[1], Axel Mithöfer[2], Erich Glawischnig[3]*, Elisabeth Georgii[1], Andrea Ghirardo[4], Basem Kanawati[5], Philippe Schmitt-Kopplin[5], Jörg-Peter Schnitzler[4], Jörg Durner[1], Frank Gaupels[1]

[1]Institute of Biochemical Plant Pathology, Helmholtz Zentrum München, German Research Center for Environmental Health, Ingolstädter Landstraße 1, D-85764 Neuherberg, Germany
[2]Max Planck Institute for Chemical Ecology, Department Bioorganic Chemistry, Hans-Knöll-Straße 8, D-07745 Jena, Germany
[3]Department of Plant Sciences, Technical University of Munich, Emil-Ramann-Str.4, D-85354, Freising, Germany
[4]Research Unit Environmental Simulation, Institute of Biochemical Plant Pathology, German Research Center for Environmental Health, Ingolstädter Landstraße 1, D-85764 Neuherberg, Germany
[5]Analytical BioGeoChemistry, Helmholtz Zentrum München, German Research Center for Environmental Health, D-85764 Neuherberg, Germany

*Present address: Chair of Chemistry of Biogenic Resources, Technical University of Munich - Campus Straubing for Biotechnology and Sustainability, Schulgasse 16, D-94315 Straubing, Germany

**One sentence summary:** Fumigation of Arabidopsis with the gaseous signaling molecule $NO_2$ triggers basal pathogen resistance that is dependent on early callose deposition.

***Authors' contributions:***

*D.M., F.G., J.D., P.S-K., and J-P.S. planned and designed the research. D.M., A.M., E.Gl., A.G., B.K., and F.G. performed the research. E.Ge.*, *D.M.*, and *B.K. analyzed the data. F.G., D.M., and J.D. wrote the manuscript with contributions from all the authors.*

***Corresponding author:** Frank Gaupels, frank.gaupels@helmholtz-muenchen.de

## ABSTRACT

Nitrogen dioxide ($NO_2$) forms in plants under stress conditions, but little is known about its physiological functions. Here, we explored the physiological functions of $NO_2$ in plant cells using short-term fumigation of Arabidopsis (*Arabidopsis thaliana*) for 1 h with 10 parts per million (ppm) $NO_2$. Although leaf symptoms were absent, the expression of genes related to pathogen resistance was induced. Fumigated plants developed basal disease resistance, or pattern-triggered immunity (PTI), against the necrotrophic fungus *Botrytis cinerea* and the hemibiotrophic bacterium *Pseudomonas syringae*. Functional salicylic acid (SA) and jasmonic acid (JA) signaling pathways were both required for full expression of $NO_2$-induced resistance against *B. cinerea*. An early peak of SA accumulation immediately after $NO_2$ exposure was followed by transient accumulation of oxophytodienoic acid. Simultaneous $NO_2$-induced expression of genes involved in jasmonate biosynthesis and jasmonate catabolism resulted in the complete suppression of JA and JA-isoleucine (JA-Ile) accumulation, which was accompanied by a rise in the levels of their catabolic intermediates 12-OH-JA, 12-OH-JA-Ile, and 12-COOH-JA-Ile. $NO_2$-treated plants emitted the volatile monoterpene α-pinene and the sesquiterpene longifolene (syn. junipene), which could function in signaling or direct defense against pathogens. $NO_2$-triggered *B. cinerea* resistance was dependent on enhanced early callose deposition and *CYTOCHROME P450 79B2* (*CYP79B2*), *CYP79B3*, and *PHYTOALEXIN DEFICIENT 3* (*PAD3*) gene functions but independent of camalexin, *CYP81F2*, and 4-OH-indol-3-ylmethylglucosinolate derivatives. In sum, exogenous $NO_2$ triggers basal pathogen resistance, pointing to a possible role for endogenous $NO_2$ in defense signaling. Additionally, the study revealed the involvement of jasmonate catabolism and volatiles in pathogen immunity.


## INTRODUCTION

Plants face many challenges from phytopathogenic bacteria, fungi, and oomycetes. These pathogenic organisms have evolved various feeding strategies. Biotrophic pathogens such as powdery mildew nourish on nutrients from living cells, while necrotrophic pathogens such as *Botrytis cinerea* kill the host to feed on dead cell contents (Glazebrook, 2005; Mengiste, 2012). Hemibiotrophs including *Pseudomonas syringae* on the other hand, can pursue both feeding strategies (Glazebrook, 2005).

The plant perceives the invading pathogen by recognizing conserved pathogen- and damage-associated molecular patterns (PAMPs and DAMPs) including the bacterial flagellin, fungal chitin, and oligogalacturans (OGs) derived from damaged plant cell walls (Boller and Felix, 2009; Heil and Land, 2014). Binding of such elicitors to specific pattern-recognition receptors (PRRs) initiates PAMP-triggered immunity (PTI) also referred to as basal pathogen

resistance (Boller and Felix, 2009; Couto and Zipfel, 2016). Immediate cellular responses upon PAMP-recognition are the rapid influx of calcium ions ($Ca^{2+}$) into the cytosol and the production of reactive oxygen species (ROS) such as superoxide ($O_2^-$) or hydrogen peroxide ($H_2O_2$) (Boller and Felix, 2009; Bigeard et al., 2015). Additionally, reactive nitrogen species (RNS), such as nitric oxide (NO), are crucial for pathogen-induced signal transduction (Gaupels et al., 2011; Mur et al., 2013).

The phytohormones salicylic acid (SA), jasmonic acid (JA), and the bioactive JA-isoleucine (JA-Ile) conjugate are considered to be major mediators of plant defense (Browse, 2009; Vlot et al., 2009; Pieterse et al., 2012; Wasternack and Hause, 2013). NONEXPRESSOR OF PR GENES 1 (NPR1) and CORONATINE INSENSITIVE 1 (COI1) are central transcriptional regulators of SA- and JA-responsive genes, respectively. The SA and JA/ET pathways are interconnected via complex regulatory networks and commonly antagonize each other with SA being a potent antagonist of JA-signaling (Robert-Seilaniantz et al., 2011; Caarls et al., 2015). Several NPR1-regulated TGA and WRKY transcription factors have been implicated in SA/JA crosstalk (Pieterse et al., 2012; Caarls et al., 2015). The JA pathway is also controlled on the level of jasmonate catabolism. In response to wounding and pathogen attack, excess JA and JA-Ile are inactivated by hydroxylation and carboxylation, forming 12-OH-JA, 12-OH-JA-Ile, and 12-COOH-JA-Ile (Heitz et al., 2016; Caarls et al., 2017; Smirnova et al., 2017). The jasmonate catabolism pathway is inducible by JA in the course of a negative feed-back regulation (Caarls et al., 2017).

Pathogens can be prevented from spreading by PAMP-triggered formation of the (1,3)-β-glucan polymer callose, which is deposited between the plasma membrane and cell wall at infection sites (Luna et al., 2011; Ellinger and Voigt, 2014). Callose deposition is induced after *B. cinerea* infection of Arabidopsis (*Arabidopsis thaliana*) (García-Andrade et al., 2011). PMR4 (POWDERY MILDEW RESISTANT 4) is the predominant callose synthase during pathogen infection (Jacobs et al., 2003; Nishimura et al., 2003; Ellinger et al., 2013). Other well-studied component of the plants arsenal against pathogens are indole glucosinolates and the phytoalexin camalexin (3-thiazol-2'yl-indole) found in Arabidopsis (Glawischnig, 2007). *In planta*, camalexin is synthesized upon detection of various PAMPs and DAMPs (Kliebenstein et al., 2005; Rauhut et al., 2009; Ahuja et al., 2012), and its antimicrobial activity against *P. syringae* and *B. cinerea* has been confirmed *in vitro* (Rogers et al., 1996; Kliebenstein et al., 2005). Indole glucosinolates such as 4-OH-indol-3-ylmethylglucosinolate (4-OH-I3M) have important functions in antifungal defense after activation by the P450 monoxygenase CYP81F2 and the atypical myrosinase PENETRATION RESISTANCE 2 (PEN2) (Bednarek et al., 2009; Clay et al., 2009).

The RNS nitrogen dioxide ($NO_2$) arises during stress-induced signaling by the oxidation of NO, reduction of nitrite ($NO_2^-$), or decomposition of peroxynitrite ($ONOO^-$) (Pryor, 2006; Groß et al., 2013). Chloroplastic nitrite reductase activity utilizes electrons diverted from photosynthesis for the multi-step reduction of nitrite to ammonia (Beevers and Hageman, 1969). Accordingly, treatment of soybean (*Glycine max*) with a photosynthesis-inhibiting herbicide or incubation in darkness leads to the accumulation of nitrite and the subsequent emission of $NO_2$ that is derived from nitrite by an unknown mechanism (Klepper, 1979; Klepper, 1990). *In vitro* experiments demonstrate that the heme-containing horseradish peroxidase (HRP) can produce $NO_2$ through one-electron reduction of nitrite in the presence of $H_2O_2$ (Shibata et al., 1995; Sakihama et al., 2003). Additionally, HEMOGLOBIN 1 of Arabidopsis and alfalfa *(Medicago sativa*) can produce $NO_2$ mechanistically similar to HRP (Sakamoto et al., 2004; Maassen and Hennig, 2011).

$NO_2$ is a highly reactive compound that can exert specific physiological functions by nitration (-$NO_2$ group) of nucleophiles such as fatty acids (FAs), nucleotides, and proteins. The nitration of FAs (nitro-FAs) has been observed in Arabidopsis exposed to abiotic stresses (Mata-Pérez et al., 2016b); and nitro-FAs are proposed to act as signaling molecules (Schopfer et al., 2011; Mata-Pérez et al., 2016b). Nitration of cyclic guanosine monophosphate (cGMP) to give 8-nitro-cGMP triggers stomatal closure whereas unmodified cGMP mediates stomatal opening (Joudoi et al., 2013). Moreover, increased protein tyrosine nitration is a common event during plant defense responses (Arasimowicz-Jelonek and Floryszak-Wieczorek, 2011; Gaupels et al., 2011; Mata-Pérez et al., 2016; Kolbert et al., 2017). This protein modification is mediated directly by $NO_2$ or via decomposition of peroxynitrite to $NO_2$, which subsequently binds to accessible protein tyrosine residues (Pryor, 2006; Radi, 2012; Groß et al., 2013; Kolbert et al., 2017). $NO_2$-modified proteins are often irreversibly inhibited as described for several antioxidant enzymes and the abscisic acid receptor PYRABACTIN RESISTANCE1 (PYR1)/PYR1-LIKE (PYL)/REGULATORY COMPONENTS OF ABA RECEPTORS (RCAR) (Gaupels et al., 2011; Groß et al., 2013; Castillo et al., 2015; Mata-Pérez et al., 2016a). Together, these examples illustrate how $NO_2$ can participate in defense signaling. On the other hand, high endogenous levels of RNS can also result in excessive oxidation and nitration of bio-molecules, severe metabolic perturbations, and even structural injuries of cells (Corpas and Barroso, 2013; Groß et al., 2013). Dependent on the severity of the inflicted nitro-oxidative stress, cells either trigger defense and repair mechanisms or die (Thomas et al., 2008; Groß et al., 2013). In this scenario, $NO_2$ and other RNS would act as inducers of defense signaling rather than signals themselves.

To date, the investigation of $NO_2$ *in vivo* is hampered by the fact that no specific dyes and donors are commercially available. For this reason, nothing is known about endogenous levels of $NO_2$ under stress conditions. Nevertheless, functions of $NO_2$ in plants have been frequently explored by fumigations with gaseous $NO_2$ as a donor treatment. After stomatal uptake, the lipophilic $NO_2$ and its more water-soluble dimer $N_2O_4$ readily penetrate cell membranes and diffuse into the cytosol (Wellburn, 1990). In the aqueous environment of the leaf $NO_2$ disproportionates to nitrite and nitrate that are further reduced to ammonia by nitrite and nitrate reductases (Beevers and Hageman, 1969; Zeevaart, 1976; Sparks, 2009). Nitrite levels are positively correlated with $NO_2$-induced leaf damage in a number of plant species (Zeevaart, 1976; Kasten et al., 2016). Plants generally accumulate high nitrite levels and show strong leaf damage after $NO_2$ fumigation in the dark (Zeevaart, 1976; Yoneyama and Sasakawa, 1979; Shimazaki et al., 1992) because - as mentioned above - nitrite reductase activity is dependent on photosynthesis. However, nitrite levels also strongly increase in pea (*Pisum sativum*) and Arabidopsis after $NO_2$ fumigation in the light probably because they exceed the enzymatic capacity of nitrite reductase (Zeevaart, 1976; Kasten et al., 2016).

Long-term exposure to parts per billion (ppb) levels of $NO_2$ has beneficial effects on plant growth and development (Srivastava et al., 1994; Takahashi et al., 2014), whereas $NO_2$ concentrations in the parts per million (ppm) range cause the induction of antioxidant defense and other stress responses (Xu et al., 2010; Liu et al., 2015; Kasten et al., 2016). In the current work, Arabidopsis was exposed to 10 ppm $NO_2$ for 1 h, which did not cause visible leaf symptoms or ion leakage as a measure of membrane damage (Kasten et al., 2016). Responses of Arabidopsis to $NO_2$ were investigated by microarray analysis, pathogen assays, and measurements of phytohormones, volatiles, camalexin, and callose.

## RESULTS

### $NO_2$ triggers the expression of genes related to pathogen defense

Exposure of Arabidopsis Col-0 plants to 10 ppm $NO_2$ for 1 h did not cause visible symptoms (Supplemental Fig. S1), which is in agreement with previous data showing that ion leakage as a measure of membrane damage does not increase after this treatment (Kasten et al., 2016). However, close examination under UV light revealed the emission of red chlorophyll fluorescence immediately after fumigation that faded at the 6 h time point (Fig. 1 A) indicative of photoprotective energy dissipation due to a transient stress-induced metabolic perturbation (Lichtenthaler and Miehe, 1997; Chaerle and Van Der Straeten, 2000).

Microarray analysis was performed with leaf material sampled immediately or 6 h after fumigation with air or 10 ppm $NO_2$ for 1 h (Supplemental Dataset S1). Volcano plots illustrated that both up- and down-regulation of gene expression was more pronounced directly after $NO_2$ fumigation than after 6 h (Fig. 1 B). Approximately 4400 genes were significantly regulated immediately after fumigation, whereas 6 h later only 1430 genes were differentially regulated (Fig. 1 C). The regulated genes scarcely overlapped among both time points (Fig. 1 B). Only 11.5% of all up- and 2.1% of all down-regulated genes were affected at both time points, which suggested discrete time-dependent responses of the plant to $NO_2$.

Gene Ontology (GO) term enrichment analysis (Supplemental Fig. S2) was applied to assess biological processes underlying the observed $NO_2$-induced gene regulation. Directly after fumigation 122 GO-terms were significantly enriched in the up-regulated gene set (Supplemental Dataset S1). The majority of GO terms was related to plant defense including responses to wounding, the fungal elicitor chitin, and fungal as well as bacterial pathogen attacks (Fig. 2 A). $NO_2$ also activated genes involved in the JA and ethylene signaling pathways, camalexin biosynthesis, flavonoid glucuronidation, and programmed cell death. Principal component analysis (PCA) was used for comparison of the $NO_2$-regulated genes to previously published microarray datasets obtained after treatment of plants with *B. cinerea* (Ferrari et al., 2007), *P. syringae* (Lewis et al., 2015), chitin (Ramonell et al., 2005), the bacterial elicitor flg22 (Zipfel et al., 2004; Boudsocq et al., 2010), and exposure to the abiotic stresses drought and/or heat (Georgii et al., 2017) (Fig. 2 B). Although the biotic stress studies were conducted on a different microarray platform (Affymetrix ATH1), their post-treatment expression samples are closer to the $NO_2$-fumigated samples directly after treatment ("$NO_2$ 0h") than the abiotic stress samples sharing the same platform with the $NO_2$ study (Agilent At8x60K, ID: 29132).

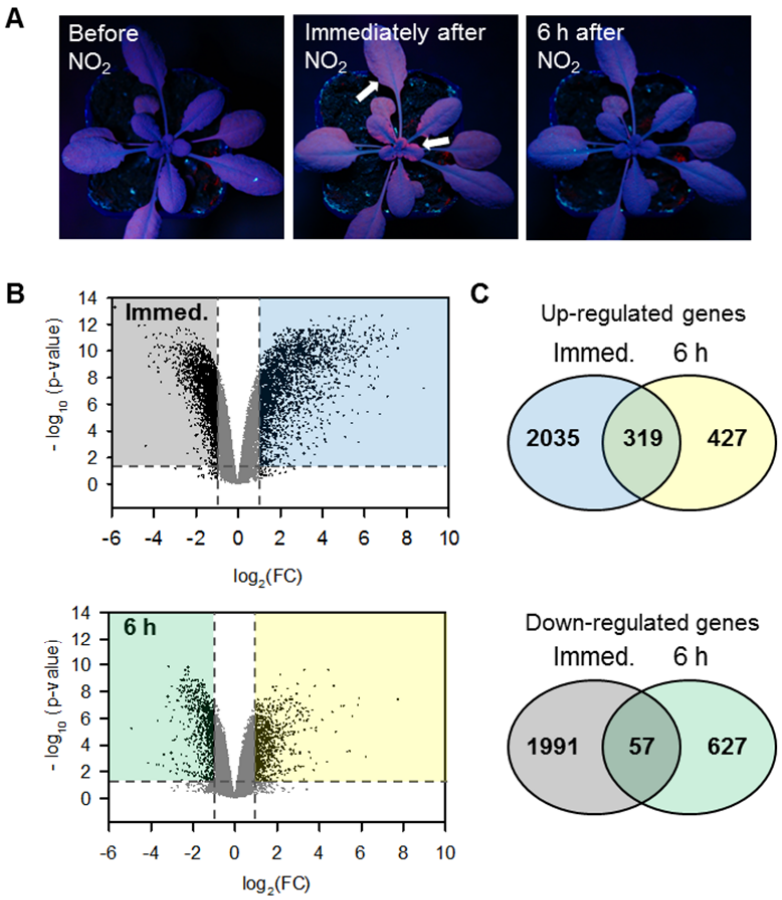


**Figure 1.** $NO_2$ triggers a rapid and transient defense response. Arabidopsis Col-0 plants were fumigated with 10 ppm $NO_2$ or air for 1 h. A, $NO_2$ caused no visible leaf damage (see also Supplemental Fig. S1) but a transient increase in red chlorophyll autofluorescence under UV light (white arrows) indicative of stress-induced photoprotective energy dissipation. B, Leaf material was harvested in quadruplicates for microarray analysis immediately or 6 h after fumigation. Volcano plots visualizing the changes in gene expression at 0 h and 6 h after fumigation by plotting the adjusted *p*-value over the fold change. Horizontal dashed lines mark $p = 0.05$; vertical dashed lines indicate $\log_2(FC) \pm 1$. Data points represent expression of individual genes. The expression of genes appearing in the colored left panels was significantly down-regulated ($p < 0.05$, $\log_2(FC) < -1$), whereas expression of genes within the colored right panels showed significant up-regulation ($p < 0.05$, $\log_2(FC) > 1$). C, Venn diagrams illustrating the number of genes that were significantly up- (top) or down-regulated (bottom) after $NO_2$ exposure with $p < 0.05$ and $\log_2(FC) \pm 1$. Color code is consistent in B and C indicating genes down-regulated immediately (grey), and 6 h (green) after fumigation or up-regulated immediately (blue) and 6 h (yellow) after fumigation.

In summary, the microarray analysis revealed that exposure to 10 ppm $NO_2$ specifically up-regulated the expression of genes associated with defense against fungal and bacterial pathogens.

**$NO_2$ triggers basal pathogen resistance**

To investigate whether $NO_2$ induces resistance against necrotrophic fungi as suggested by the gene expression data, $NO_2$ fumigated plants were infected with *B. cinerea*. Arabidopsis Col-0 plants were fumigated with 10 ppm $NO_2$ for 1 h, followed by droplet-infection of detached leaves with *B. cinerea* 6 h later. The areas of the developing necrotic lesions were

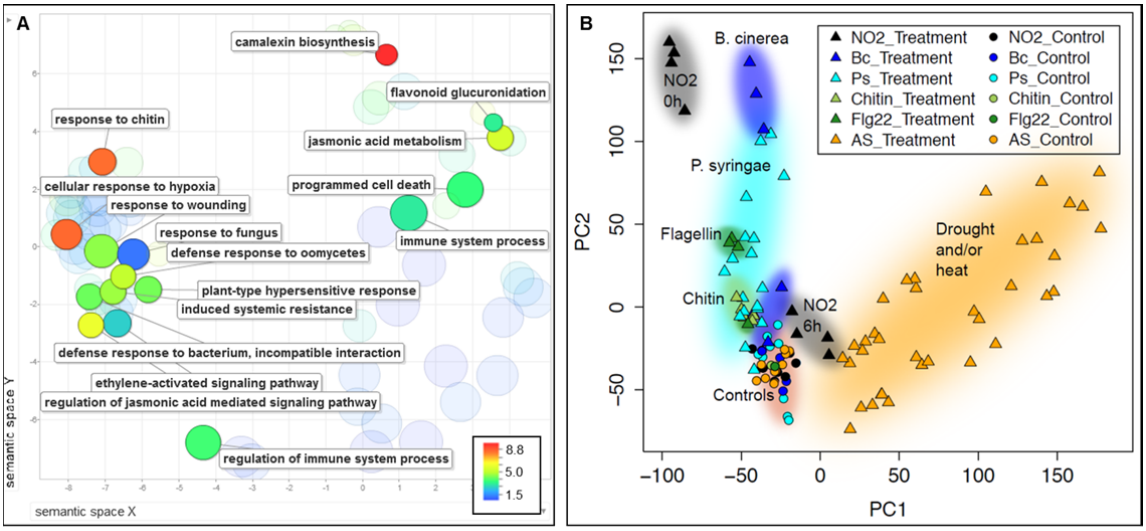


**Figure 2.** $NO_2$–induced genes are related to pathogen defense. A, GO term enrichment of genes up-regulated directly (0 h) after fumigation. Enriched GO terms ($p < 0.05$) were identified using the PANTHER 11.0 overrepresentation test and visualized in scatter plots using the REVIGO tool. Each circle represents a GO term, and circle size represents the number of genes encompassed. The color code depicts the fold enrichment of the respective GO term within the data set compared to the PANTHER Arabidopsis reference list. Circles are clustered according to the distance of the respective GO terms within the GO hierarchical tree. Highly enriched or interesting GO terms were labeled. B, Principal component analysis of Arabidopsis gene expression responses to $NO_2$ fumigation, biotic stress, and abiotic stress. Data from microarray analysis after $NO_2$ fumigation were combined with previously published datasets representing responses to different stresses and elicitors (115 samples in total). The overall expression response similarities between samples of the combined dataset are visualized using the top two principal components (PCs), capturing 22% and 14% of the total variation, respectively. NO2, $NO_2$ fumigation; Bc, *Botrytis cinerea* infection, ArrayExpress accession number E-GEOD-5684; Ps, *Pseudomonas syringae* infection, E-GEOD-6176; Chitin, Chitin treatment, E-GEOD-2538; flg22, flagellin epitope 22 treatment, E-GEOD-17382; AS: abiotic stress treatment study, E-MTAB-4867; for each study, treated samples are marked by triangles and controls by circles.

then analyzed to assess if $NO_2$ provides resistance against this pathogen. In Fig. 3 A, a representative example of the necrotic lesions formed on $NO_2$-fumigated and non-treated plants is illustrated. Quantification of the necrotic areas revealed that the average sizes of necrotic lesions formed on $NO_2$ fumigated leaves were significantly reduced by ~30% when compared to unfumigated leaves (Fig. 3 A). Therefore, these results confirmed that $NO_2$ induces resistance against the necrotrophic fungus *B. cinerea*.

The GO term enrichment analysis and PCA suggested that $NO_2$ also elicits defense responses effective against bacterial pathogens. Therefore, plants were fumigated with $NO_2$, followed by syringe infiltration with $1x10^5$ colony forming units per ml (cfu $ml^{-1}$) *P. syringae* pv. *tomato* DC3000 4 h later. The bacterial titers in the infected leaves were determined 2 h, 1 day, and 2 days post infection (dpi) to determine if $NO_2$ fumigation influenced bacterial growth. As shown in Fig. 3 B, infected leaves pretreated with 10 ppm $NO_2$ harbored fewer bacteria than their unfumigated counterparts. Therefore, it can be concluded that $NO_2$-induced signaling also decreased the susceptibility of Arabidopsis to the hemi-biotrophic bacterium *P. syringae*.

Together, the findings above imply that $NO_2$ initiated the onset of basal pathogen resistance similar to the induction of PTI by PAMPs such as chitin and flagellin.

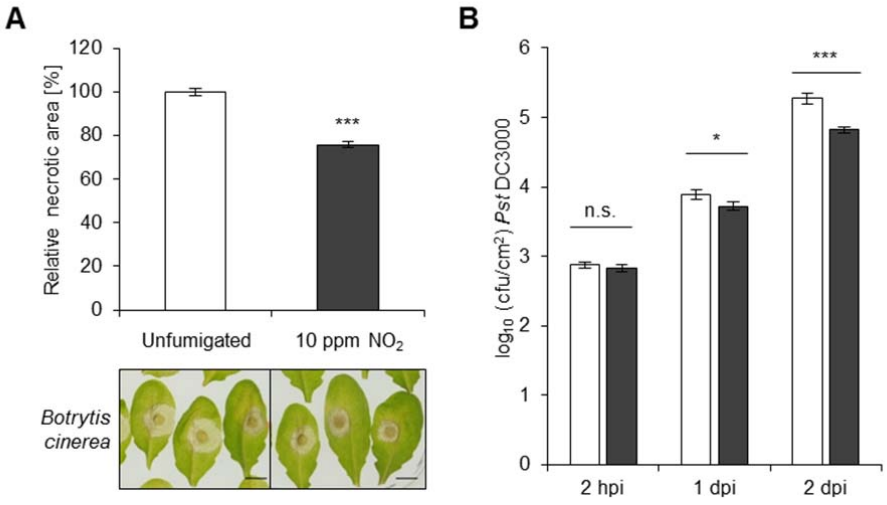


**Figure 3.** $NO_2$ induces resistance against *B. cinerea* and *P. syringae*. A, Col-0 plants were fumigated or not (control) with 10 ppm $NO_2$ for 1 h, followed by droplet-infection of detached leaves with approx. 1000 spores of *B. cinerea* 6 h after fumigation. Necrotic lesion area was measured 3 days later using ImageJ. Columns represent means of 18 independent experiments ± SE; n = 624-640. Asterisks indicate significant differences from control according to the Mann Whitney Rank Sum Test (***$p < 0.001$). Representative photographs of necrotic lesions 3 days after droplet-infection with *B. cinerea* are shown. Scale = 5 mm. B, Col-0 plants were fumigated with 10 ppm $NO_2$ for 1 h and syringe-infiltrated with $1x10^5$ cfu/ml *P. syringae* pv. *tomato* DC3000 4 h after fumigation. Leaf discs from infected leaves were obtained 2 hours or 1 and 2 days after infection to determine the bacterial titer (cfu/$cm^2$ leaf material). Columns represent means ± SE from 7 independent experiments; n (2 hpi) = 26-27, n (1 dpi) = 72, n (2 dpi) = 66. Asterisks indicate significant differences of all pairwise comparisons via Two Way ANOVA plus Holm-Sidak post-hoc Test (*$p < 0.05$, ***$p < 0.001$). hpi, hours post infection; dpi, days post infection; cfu, colony forming units; n.s., not significant; white columns, unfumigated; black columns, 10 ppm $NO_2$.

## $NO_2$ triggers signaling by SA and oxophytodienoic acid (OPDA) while JA and JA-Ile are catabolized

SA biosynthesis and signaling genes were enhanced following $NO_2$ exposure (Supplemental Dataset S1, Supplemental Fig. S3). Therefore, levels of this hormone were determined by LC-MS/MS after fumigation with 10 ppm $NO_2$ (Fig. 4). SA levels were approximately 90 ng $g^{-1}$ fresh weight (FW) in air fumigated leaves when averaged across time points but increased to 121 and 133 ng $g^{-1}$ FW directly or 3 h after fumigation with $NO_2$, respectively. At the 6 h time point the SA content rapidly declined again to 73 ng $g^{-1}$ FW, resulting in a significant decrease of 31% when compared to the concentration in the respective air-fumigated control. This is in line with the observation that transcript levels of the biosynthetic genes declined at this time point as well (Supplemental Dataset S1). In summary, exposure to 10 ppm $NO_2$ provoked a rapid, but transient accumulation of SA.

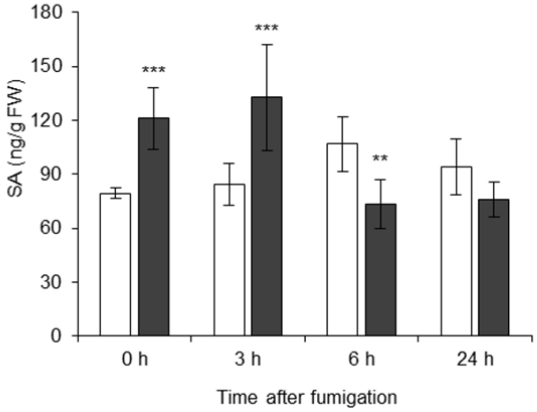


**Figure 4.** $NO_2$ induces signaling by SA. SA levels at different time points after fumigation with air or 10 ppm $NO_2$ were measured via LC-MS/MS and normalized to the samples' fresh weight (FW). Columns represent means ± SD; n = 5. Asterisks indicate significant differences within the time points as determined by Two Way ANOVA plus Holm-Sidak post-hoc Test (**$p$ < 0.01,***$p$ < 0.001). White columns, air; black columns: 10 ppm $NO_2$.

Jasmonates derive from the fatty acid linolenic acid which undergoes oxidation via lipoxygenases (LOX), dehydration via the allene oxide synthase (AOS), followed by subsequent cyclization to OPDA via the allene oxide cyclases (AOC). After *cis*-OPDA is reduced by OPDA-reductase (OPR3), three rounds of β-oxidation (e.g. via Acyl-CoA oxidase (ACX1) and OPC-8:0 CoA ligase (OPCL1)) are necessary to form JA. JA in turn, can be modified to JA-Ile or methyl JA via jasmonate-amido synthetase (JAR1) and JA-carboxyl methyltransferase (JMT), respectively (Browse, 2009; Wasternack and Hause, 2013). This biosynthetic pathway is outlined in Fig. 5. The majority of depicted genes were significantly up-regulated directly after fumigation with a $\log_2$(FC) of up to 5.9 for *AOC3*, whereas 6 h after fumigation the expression levels generally declined.

A major step during the catabolic turnover of active jasmonates is the oxidation of JA-Ile by members of the cytochrome P450 94 (CYP94) family (Fig. 5) resulting in biologically inactive 12-OH-JA-Ile and 12-COOH-JA-Ile (Kitaoka et al., 2011; Koo et al., 2011; Heitz et al., 2012). JA-Ile and its hydroxylated form can be further catabolized to tuberonic acid (12-OH-JA) by the amidohydrolases IAA-ALANINE RESISTANT 3 (IAR3) and IAA-LEUCINE RESISTANT (ILR)-LIKE 6 (ILL6) (Widemann et al., 2013). Moreover, jasmonate-induced oxygenases (JOXs) hydroxylate JA to its inactive 12-OH-JA derivative (Caarls et al., 2017; Smirnova et al., 2017), which represents yet another pathway of jasmonate catabolism. Directly after fumigation, the majority of genes involved in these catabolic reactions were highly up-regulated with fold changes to the respective air controls ranging from $\log_2$(FC) 1.3 up to 7.4. The genes encoding for the CYP94 enzymes and members of the JOXs were highly induced.

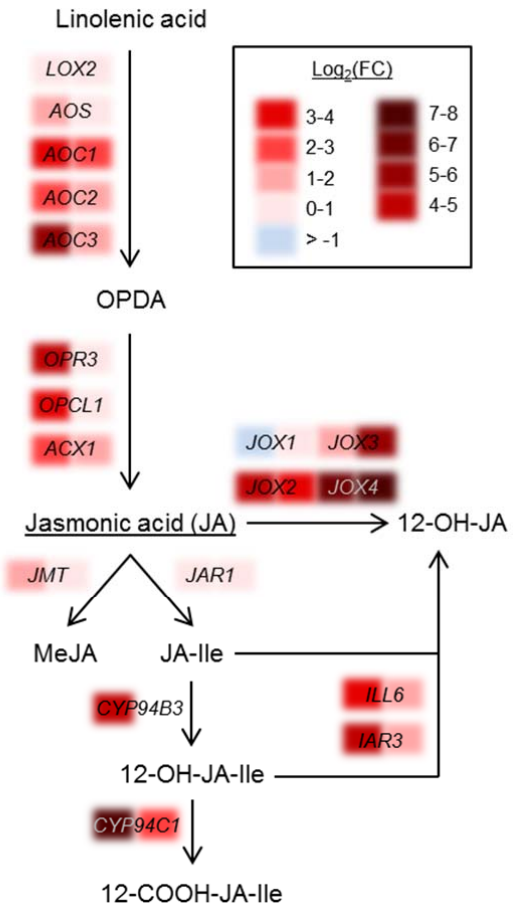


**Figure 5.** JA biosynthesis and degradation pathways are simultaneously up-regulated in response to $NO_2$. Schematic pathway of jasmonate metabolism illustrating the change in expression levels ($log_2$(FC)) of the respective genes obtained from the microarray analysis immediately (0 h, left part of colored panel) or 6 h (right part of colored panel) after fumigation with 10 ppm $NO_2$. Expression levels of all depicted genes can be found in Table S1. JA, jasmonic acid; OPDA, *cis*-(+)-12-oxophytodienoic acid; JA-Ile, jasmonoyl-L-isoleucine; MeJA, methyl jasmonate; 12-OH-JA, tuberonic acid; 12-OH-JA-Ile, hydroxyl-JA-Ile; 12-COOH-JA-Ile, dicarboxy-JA-Ile.

The transcript levels of JOXs were still significantly elevated up to a $log_2$(FC) of 7.8 6 h after $NO_2$ treatment. Besides the JOXs, the gene transcripts of most of the above mentioned catabolic enzymes were also still highly abundant at this time point after fumigation. All expression levels of the depicted genes can be found in Supplemental Dataset S1.

The gene expression data suggested the simultaneous induction of jasmonate biosynthesis and catabolism. LC-MS/MS revealed that OPDA levels were elevated by 69% at 6 h after fumigation compared to leaf extracts from air-fumigated plants (Fig. 6 A), which was associated with the enhanced expression of defensin-coding genes including *PLANT DEFENSIN 1.2A* (*PDF1.2A*) (Supplemental Dataset S1). By contrast, significant changes were neither detected for JA nor JA-Ile (Fig. 6 B,C). The rapid and extensive $NO_2$-induced

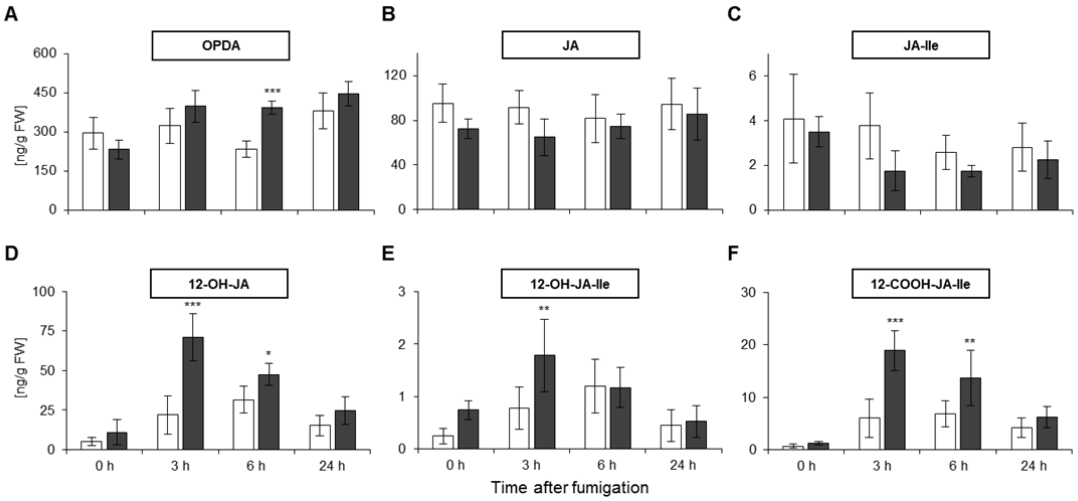


**Figure 6.** JA degradation products accumulate in response to $NO_2$. Various jasmonates were measured by LC-MS/MS at different time points after fumigation with air or 10 ppm $NO_2$. Concentrations were normalized to the leaf sample fresh weight (FW). A, OPDA, *cis*-(+)-12-oxophytodienoic acid; B, JA, jasmonic acid; C, JA-Ile, jasmonoyl-L-isoleucine; D, 12-OH-JA, tuberonic acid; E, 12-OH-JA-Ile; F, 12-COOH-JA-Ile. A-C, Products of JA biosynthesis pathway. D-F, JA catabolism products. Columns represent means ± SD; n = 5. Asterisks indicate significant differences within the time points according to Two Way ANOVA plus Holm-Sidak post-hoc Test (*$p$ < 0,05, **$p$ < 0.01,***$p$ < 0.001). White columns, air; black columns, 10 ppm $NO_2$.

transcription of genes whose products are necessary for jasmonate catabolism encourages the hypothesis that $NO_2$ stimulates rapid jasmonate turnover. Accordingly, all catabolic intermediates of JA and JA-Ile increased and peaked in their concentrations at 3 h after $NO_2$ fumigation. 12-OH-JA increased significantly by a factor of 3.2 from 22 ng $g^{-1}$ FW in air fumigated plants to 71 ng $g^{-1}$ FW after $NO_2$ treatment (Fig. 6 D) while 12-OH-JA-Ile levels elevated significantly by 2.3-fold at 3 h after fumigation when compared to the air fumigated control (Fig. 6 E). A 3.1-fold increase was observed for 12-COOH-JA-Ile from 6 ng $g^{-1}$ FW (air) to 19 ng $g^{-1}$ FW ($NO_2$) (Fig. 6 F). After the concentration of all intermediates peaked at 3 h after treatment, their accumulation gradually declined to base line levels 24 h after $NO_2$ treatment.

Together, the results suggest that exposure to $NO_2$ triggered consecutive peaks of SA and OPDA. The simultaneous induction of jasmonate production and catabolism pathways resulted in the accumulation of 12-OH-JA, 12-OH-JA-Ile, and 12-COOH-JA-Ile. The latter process might be controlled by genes involved in SA/JA antagonism crosstalk that were strongly up-regulated upon $NO_2$ exposure (Supplemental Dataset S1).

**The SA and JA signaling pathways are both crucial for $NO_2$-induced *B. cinerea* resistance**

Since SA biosynthesis was up-regulated upon $NO_2$ fumigation, the role of SA in the $NO_2$-induced resistance against *B. cinerea* was examined by utilizing mutants defective in *SALICYLIC ACID INDUCTION DEFICIENT 2* (*SID2*) and plants expressing the

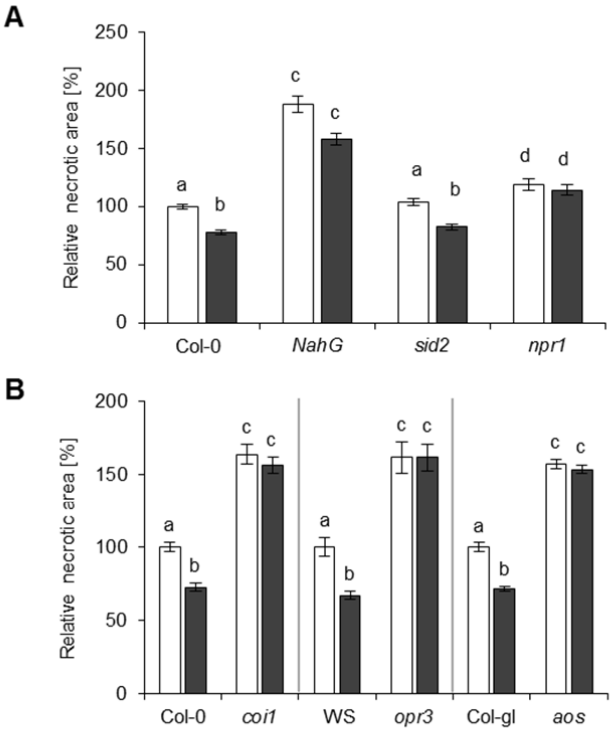


**Figure 7.** SA and JA function in $NO_2$-induced resistance against *B. cinerea*. Mutants were subjected to *B. cinerea* droplet-infection 6 h after fumigation with 10 ppm $NO_2$ for 1 h. Necrotic areas were measured 3 days later and were normalized to the mean necrotic area of the respective unfumigated wild-type. A, SA-deficient (NahG, *sid2*) or SA-signaling (*npr1*) mutants and corresponding Col-0 wild-type. Columns represent means of at least 3 independent experiments ± SE; n = 95-331. B, JA-deficient *(aos, opr3*) or JA-signaling (*coi-1*) mutants and corresponding wild-types (Col-gl for *aos*, WS for *opr3*, Col-0 for *coi-1*). Columns represent means of three independent experiments ± SE; n = 66-126. Letters indicate significant differences of all pairwise comparisons via Kruskal Wallis Test plus Dunn`s post-hoc Test ($p < 0.05$). White columns, unfumigated; black columns, 10 ppm $NO_2$.

*Pseudomonas putida NahG* gene. The *sid2* mutant is impaired in the main SA biosynthesis pathway and therefore does not accumulate SA upon pathogen infection (Nawrath and Métraux, 1999; Wildermuth et al., 2001), whereas *NahG*-transgenic plants express a bacterial SA hydroxylase that degrades SA to catechol (Delaney et al., 1994). The *B. cinerea* infection assay after $NO_2$ fumigation revealed that in Col-0 plants the lesion size was reduced by 22% upon $NO_2$-pretreatment (Fig. 7 A). The relative necrotic area of $NO_2$-fumigated *sid2* was also reduced by 18.4% when compared to the lesion size of its non-fumigated counterpart. However, $NO_2$-pretreatment provoked only a 14% reduction of the relative necrotic area of *NahG*-expressing plants. This decrease was not significantly different ($P > 0.05$) from the average lesion size measured on unfumigated *NahG* plants (Fig. 7 A) indicating that the $NO_2$-induced resistance against *B. cinerea* was compromised. Furthermore, the SA-insensitive *npr1* mutant was included in the *B. cinerea* infection assay after $NO_2$ fumigation. Interestingly, $NO_2$-pretreatment of *npr1* plants did not result in a reduction of *B. cinerea*-induced necrotic lesions. The basal resistance of unfumigated plants

was not strongly altered in *sid2* and *npr1* (+18.7% relative necrotic area compared to Col-0 in untreated trials) but was markedly compromised in *NahG* transgenic plants (+88.0% relative necrotic area). Similar results have been reported for these plant lines (Ferrari et al., 2003). Taken together, the results suggest that the $NO_2$-induced resistance against *B. cinerea* is mediated by NPR1. However, it did not require SA synthesis via SID2, whereas the degradation of SA by bacterial NahG partially abolished the $NO_2$-induced resistance phenotype.

$NO_2$ exposure caused a strong rearrangement of jasmonate metabolism. To investigate, whether jasmonates or components of the JA signaling pathway were implicated in the $NO_2$-induced pathogen resistance, several Arabidopsis knock-out mutants impaired in JA-biosynthesis and -signaling were subjected to the *B. cinerea* infection assay. The *aos* and *opr3* knock-out mutants were utilized, since they are impeded in JA accumulation upon wounding or *B. cinerea* infection (Stintzi and Browse, 2000; Park et al., 2002). As shown in Fig. 7 B, the size of the *B. cinerea*-induced lesions was not affected by $NO_2$ treatment in both JA-deficient mutants whereas the necrotic lesions on $NO_2$-treated Col-gl (*aos* parental line) were reduced by 28.6%, and WS (wild-type of *opr3*) displayed a 33.1% reduction in lesion size upon $NO_2$ fumigation. Knock-out mutants that were impaired in JA signaling were also examined for their $NO_2$-induced resistance phenotype. The JA-insensitive *coi1* mutant did not show any significant differences in the size of the necrotic lesions that developed on $NO_2$-fumigated or untreated leaves upon *B. cinerea* infection. The results indicated that the $NO_2$-induced resistance against *B. cinerea* is dependent on JA accumulation and COI1-mediated signaling. It is noteworthy that the three tested JA mutants were all more susceptible than the respective wild-type lines confirming the importance of JA in basal resistance against *B. cinerea* (Thomma et al., 1998).

Collectively, the results above argue for a crucial role of SA and jasmonates during the $NO_2$-induced pathogen resistance. However, further phytohormone measurements revealed that the levels of SA, JA, and JA-Ile at 16, 24, and 48 h after *B. cinerea* infection were not influenced by $NO_2$ pre-treatment (Supplemental Fig. S4). This would suggest that SA, OPDA, and possibly the accumulating JA/JA-Ile catabolites function in the $NO_2$-mediated induction of defense responses before but not during *B. cinerea* infection.

**The volatile organic compounds (VOCs) α-pinene and longifolene are induced after $NO_2$ exposure**

Under stress conditions plants emit a wide range of VOCs (Niinemets, 2010). Among several detected VOCs (Supplemental Fig. S5), only the emission of the monoterpene α-pinene and

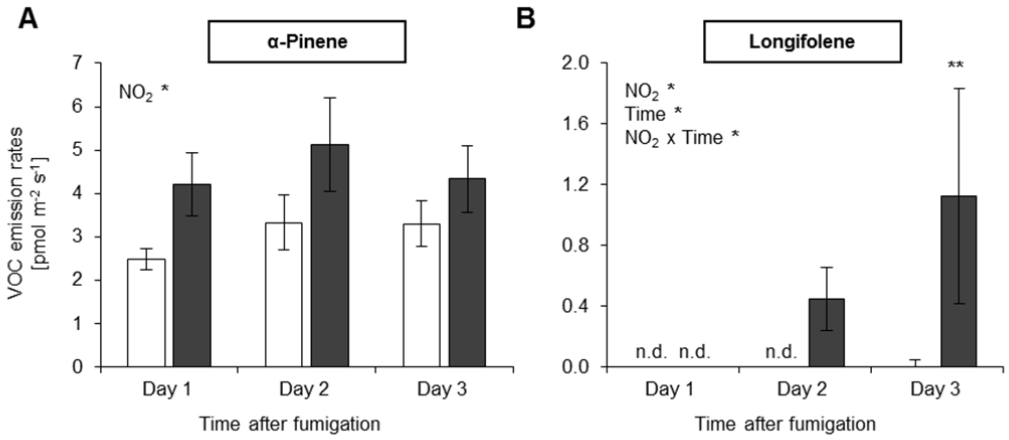


**Figure 8.** $NO_2$ exposure induces volatile emissions. A, Emission of the monoterpene α-pinene. B, Emission of the sesquiterpene longifolene. After 1 h of fumigation with 10 ppm $NO_2$, Arabidopsis Col-0 plants were enclosed in a flow-through cuvette system and volatile emissions were collected and successively analyzed by TD-GC-MS and multivariate data analysis (Supplemental Fig. S5, S6). Columns represent means ± SE; n = 10-12; Significant main effects ($NO_2$, Time) and interactions ($NO_2$ x Time) are shown (Two-Way ANOVA, all pairwise multiple comparison Holm-Sidak post-hoc test), $*p < 0.05$, $**p < 0.01$; n.d., not detected. White columns, control (air); black columns, 10 ppm $NO_2$.

the sesquiterpene longifolene were significantly increased after exposing plants to $NO_2$ (Fig. 8, Supplemental Figs. S5 and S6). α-pinene acts as a signal in the plant-to-plant communication of systemic acquired resistance (SAR) (Riedlmeier et al., 2017) while sesquiterpenes often are released after the occurrence of abiotic/biotic stress (Ghirardo et. al., 2012; Ghirardo et al., 2016). $NO_2$ induced the emission of α-pinene between 1 and 9 h (day 1) after $NO_2$ fumigation (Fig. 8 A), although the expression of the monoterpene biosynthetic gene *GERANYLGERANYL REDUCTASE* (*GGR*) was not enhanced immediately or 6 h after $NO_2$ exposure (Supplemental Dataset S1). By comparison, increases of longifolene (syn. junipene) were not detectable until the day after $NO_2$ exposure (day 2) and significantly increased ($p < 0.05$) the following day (day 3) (Fig. 8 B). The sesquiterpene related gene *CYP81D11* was found upregulated immediately after the $NO_2$ treatment (Supplemental Dataset S1). Similar to α-pinene, longifolene emission rates were very low.

**$NO_2$-induced *B. cinerea* resistance involves CYP79B2/B3 and PAD3 but not camalexin**

$NO_2$ exposure triggered the expression of genes involved in the biosynthesis of tryptophan-derived secondary metabolites (Fig. 9 A, Supplemental Dataset S1). In the initial step of this pathway, CYP79B2 and CYP79B3 convert tryptophan into indole-3-acetaldoxime, which serves as a precursor for both indole glucosinolates as well as camalexin (Hull et al., 2000; Glawischnig et al., 2004). The expression of *CYP79B2* increased immediately after $NO_2$ fumigation with a $\log_2$(FC) of 1.6 but was not strongly altered at the 6 h time point while *CYP79B3* was generally less responsive to $NO_2$ (Fig. 9A). In the indole glucosinolate

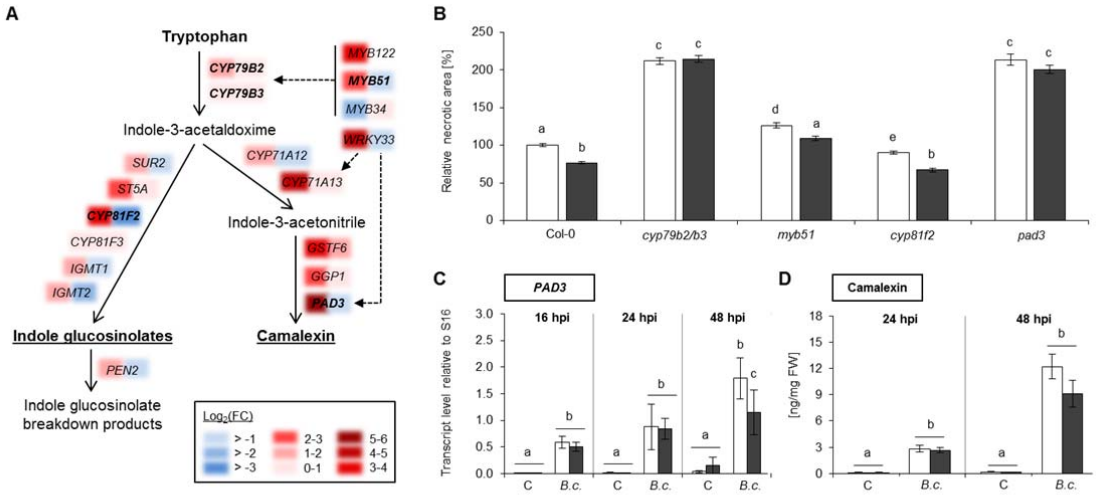


**Figure 9.** $NO_2$-induced resistance against *B. cinerea* is dependent on *CYP79B2*, *CYP79B3*, and *PAD3* but independent of camalexin. A, The expression of genes related to the biosynthesis of tryptophan-derived indole glucosinolates and camalexin was strongly up-regulated after fumigation with 10 ppm $NO_2$ for 1 h. Colored panels indicate gene expression ($log_2$(FC)) immediately (left panel) or 6 h (right panel) after the $NO_2$ treatment. Genes that were investigated further are highlighted in bold letters. Gene regulation by transcription factors is indicated by dash line arrows. B, The *cyp79b2/b3* double mutant and the *myb51*, *cyp81f2*, and *pad3* mutants were subjected to *B. cinerea* droplet-infection 6 h after fumigation with 10 ppm $NO_2$ for 1 h. Necrotic areas were measured 3 days later and were normalized to the mean necrotic area of the unfumigated Col-0 wild-type. Columns represent means of three independent experiments ± SE; n = 81-418. Letters indicate significant differences of all pairwise comparisons via Kruskal Wallis Test plus Dunn`s post-hoc Test ($p < 0.01$). C, $NO_2$-exposed or control (unfumigated) Col-0 plants were spray-infected with 2 x $10^5$ *B. cinerea* spores 6 h after fumigation. *PAD3* transcript levels were quantified 16, 24, or 48 h after infection, relative to S16 expression via RT-qPCR. Columns represent means of two independent experiments ± SD; n = 5. Letters indicate significant differences of all pairwise comparisons within the time points via Two Way ANOVA plus Holm-Sidak post-hoc Test ($p < 0.01$). D, Plants were spray-infected with *B. cinerea* at 6 h after $NO_2$- or air-fumigation. Camalexin levels were measured by HPLC-MS 24 and 48 h after infection. Columns represent means ± SE; n = 12. Letters indicate significant differences of all pairwise comparisons within the time points via Two Way ANOVA plus Holm-Sidak post-hoc Test ($p < 0.01$).

pathway, CYP81F2 and CYP81F3 catalyze the hydroxylation of indol-3-ylmethylglucosinolate (I3M, glucobrassicin) to 4-OH-I3M. The expression of *CYP81F2* was up-regulated with a $log_2$(FC) of 3.3 immediately after $NO_2$ fumigation but was down-regulated at the 6 h time point. By comparison, *CYP81F3* expression was only marginally altered after the $NO_2$ treatment. Camalexin biosynthesis is dependent on the enzyme PAD3, which synthesizes both camalexin and the precursor dihydrocamalexin (Schuhegger et al., 2006; Bottcher et al., 2009). *PAD3* expression was enhanced with a $log_2$(FC) of 5.5 immediately after $NO_2$ fumigation but dropped to wild-type levels at the 6 h time point.

The above-mentioned genes all function in plant resistance against fungal pathogens and, therefore, their possible involvement in $NO_2$-induced resistance against *B. cinerea* was further investigated using appropriate mutants. Upon *B. cinerea* infection the *cyp79b2/b3* double mutant displayed a 112% increase in necrotic area formation compared to wild-type plants, which was not influenced by pre-treatment with 10 ppm $NO_2$ 6 h before inoculation (Fig. 9 B). Hence, CYP79B2/B3 play an important role in basal and $NO_2$-induced resistance against *B. cinerea*. This conclusion was corroborated by the fact that *myb51* mutant plants lacking the MYB51 positive regulator of *CYP79B2/B3* expression were significantly more susceptible to *B. cinerea* than Col-0 wild-type plants. Upon $NO_2$ fumigation the necrotic area was reduced only by 12% as compared to 23% in Col-0 plants suggesting that the $NO_2$-induced resistance was partially compromised (Fig. 9 B).

Additional experiments with the *cyp81f2* and *pad3* mutants were aimed at determining the specific contributions of indole glucosinolates and camalexin to basal and $NO_2$-induced pathogen immunity. *B. cinerea* infection of the *cyp81f2* mutant caused necrotic lesions with 10% smaller areas than in wild-type plants. Pre-treatment with $NO_2$ before infection resulted in a 33% reduction in lesion size demonstrating that the *cyp81f2* mutant was capable of establishing $NO_2$-induced pathogen resistance (Fig. 9 B). By contrast, the camalexin-deficient *pad3* mutant displayed an enhanced susceptibility towards *B. cinerea* as reported earlier (Ferrari et al., 2003). This became apparent by the 113% increase in necrotic lesion size that developed on unfumigated *pad3* plants compared to unfumigated wild-type plants (Fig. 9 B). At 3 dpi the necrotic lesions on $NO_2$-pretreated leaves of *pad3* did not significantly differ in their size in comparison to their unfumigated control suggesting that *pad3* did not develop $NO_2$-induced *B. cinerea* immunity (Fig. 9 B). Regarding the compromised basal and $NO_2$-induced *B. cinerea* resistance, *pad3* had a similar phenotype to the *cyp79b2/b3* mutant.

These findings led us to conclude that the induction of camalexin biosynthesis genes contributed to the $NO_2$-induced resistance against *B. cinerea*. Surprisingly, however, no accumulation of camalexin was observed upon $NO_2$ exposure (Supplemental Fig. S7). Moreover, the $NO_2$ treatment did not alter *PAD3* expression or camalexin levels upon *B. cinerea* infection (Fig. 9 C,D). Reverse-transcription quantitative PCR (RT-qPCR) analysis 16 and 24 h after infection demonstrated that *PAD3* transcript levels significantly increased to the same extent upon *B. cinerea* infection in unfumigated and $NO_2$-treated Col-0 plants (Fig. 9 C). Accordingly, no statistical differences in the camalexin content of air- and $NO_2$-treated Col-0 plants were detected after *B. cinerea* infection (Fig. 9 D) although *B. cinerea* infection led to a significant gradual increase in camalexin from basal 0.1 to 12.2 ng $mg^{-1}$ FW after 48 h in $NO_2$-treated plants.

Taken together, these results indicated that $NO_2$ fumigation rapidly induced the expression of camalexin biosynthesis genes but did not result in camalexin accumulation. It was further shown that $NO_2$-induced *B. cinerea* resistance was dependent on CYP79B2/B3 and PAD3 but independent of camalexin, CYP81F2, and indole glucosinolates.

**Tryptophan-derived secondary metabolites accumulate after $NO_2$ fumigation**

Non-targeted Fourier transform ion cyclotron resonance mass spectrometry (FT-ICR-MS) was employed to identify tryptophan-derived secondary metabolites that could function as signals or defensive compounds in $NO_2$-induced *B. cinerea* resistance. To this end, Arabidopsis Col-0 plants were exposed to 10 ppm $NO_2$ for 1 h, and leaves were sampled 6 h

later because this was the time point at which plants were usually inoculated with *B. cinerea* spores. Leaf extracts from untreated *cyp79b2/b3* plants served as zero reference because they are devoid of tryptophan-derived indole glucosinolates and camalexin (Hull et al., 2000; Glawischnig et al., 2004). The following criteria were applied to filter the FT-ICR-MS results for candidate CYP79B2/B3-dependent metabolites involved in $NO_2$-induced pathogen immunity: (a) Metabolites were not detected in *cyp79b2/b3* extracts but in all 10 leaf extracts from wild-type plants and (b) showed significantly up-regulated levels at 6 h after $NO_2$ fumigation. Three of nine identified metabolites had exact masses corresponding to the indole glucosinolate glucobrassicin (I3M), its degradation product ascorbigen, and the methoxylated ascorbigen derivative 1,4-dimethoxyindol-3-ylmethylascorbate (Table 1, Supplemental Table S1) confirming that the experimental approach identified tryptophan-derived compounds. Two other metabolites contained no sulfur atom but at least one nitrogen atom and thus could represent indolic compounds. Further experiments are needed to specify if and how glucobrassicin, ascorbigen, 1,4-dimethoxyindol-3-ylmethylascorbate, and the other identified CYP79B2/B3-dependent metabolites are involved in $NO_2$-induced *B. cinerea* immunity.

**Enhanced callose formation is essential for $NO_2$-induced *B. cinerea* resistance**

Callose deposition at infection sites is an effective plant defense mechanism against various pathogens (Ellinger and Voigt, 2014). The *pmr4* mutant is defective in the *GLUCAN SYNTHASE-LIKE 5* (*GSL5*) gene and does not deposit callose upon pathogen infection (Jacobs et al., 2003; Nishimura et al., 2003). This mutant was subjected to the *B. cinerea* infection assay after $NO_2$ fumigation (Fig. 10 A). The size of necrotic lesions did not differ between $NO_2$-treated and unfumigated *pmr4* plants, whereas the $NO_2$-treated Col-0 wild-type exhibited a 23.7% reduction of the necrotic area. Additionally, Col-0 leaves were infiltrated with the callose deposition inhibitor 2-deoxy-D-glucose (2-DDG) (Bayles et al., 1990) or $H_2O$ 24 h before $NO_2$-treatment, followed by *B. cinerea* droplet-infection 6 h after fumigation (Fig. 10 B). $H_2O$-infiltrated plants developed a 31% lesion size reduction when compared to the lesions formed on unfumigated, non-infiltrated leaves. Importantly, $NO_2$-induced resistance was suppressed in $NO_2$-fumigated, 2-DDG treated leaves (Fig. 10 B). Hence, PMR4-mediated callose deposition is essential for $NO_2$-induced resistance.

Autofluorescence of *B. cinerea* interfered with the Aniline Blue staining of callose. Therefore, chitosan was employed as a potent elicitor of callose deposition (Kohle et al., 1985). Arabidopsis Col-0 plants were fumigated with $NO_2$ followed by leaf infiltration of 500 µg $ml^{-1}$ chitosan 4 h later (Fig. 11). The photometric Aniline blue assay revealed that chitosan triggered a 4- to 6-fold increase in fluorescence at 4 and 16 h after the elicitor treatment,

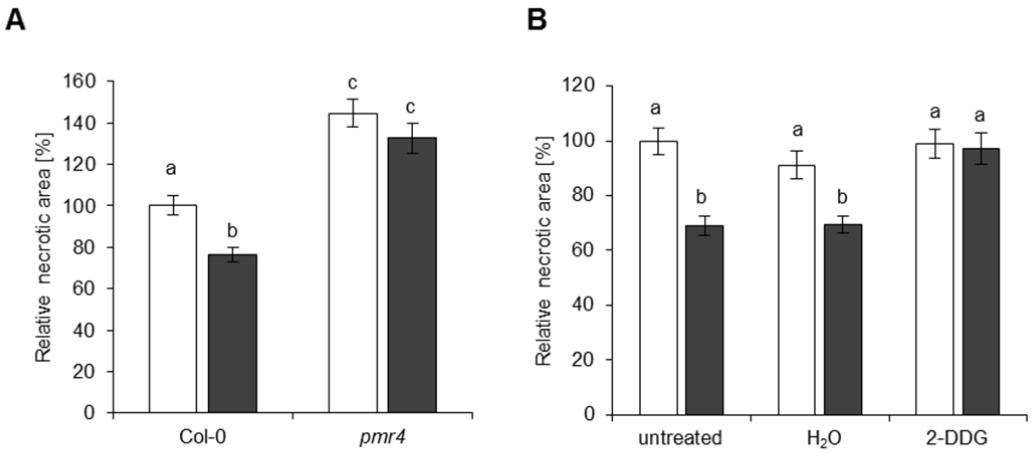


**Figure 10.** Plants impaired in callose formation display a loss in $NO_2$-induced resistance against *B. cinerea*. A, Col-0 and callose-deficient *pmr4* plants were subjected to *B. cinerea* droplet-infection 6 h after fumigation with 10 ppm $NO_2$ for 1 h. Necrotic areas formed on fumigated leaves after 3 days were normalized to the mean necrotic area of the respective unfumigated leaves. Columns represent means of four independent experiments ± SE; n = 135-145. B, Relative necrotic area determined on Col-0 plants that were infiltrated with 1.2 mM of the callose-synthesis inhibitor 2-DDG ($H_2O$ as control) 24 h before fumigation followed by *B. cinerea* infection. Columns represent means ± SE; n = 70-130. (a, b) Letters indicate significant differences of all pairwise comparisons via Kruskal Wallis Test plus Dunn`s post-hoc Test ($p < 0.05$). 2-DDG, 2-deoxy-D-glucose; white columns, unfumigated; black columns, 10 ppm $NO_2$.

510 respectively (Fig. 11 A). Exclusively at the earlier time point the callose-dependent
511 fluorescence was further enhanced in $NO_2$-pretreated plants. Aniline blue fluorescence was
512 localized in the extracellular space but was absent in *pmr4* confirming the specificity of the
513 callose detection (Fig. 11 B). The $NO_2$-enhanced callose formation at 4 h after chitosan
514 treatment was suppressed in the SA mutants *npr1* and *sid2* and in the JA signaling mutant
515 *coi1* although the chitosan-induced callose formation was observed in all mutants (Fig. 11 C).
516 As expected, almost no chitosan-induced callose formation was detected in the *pmr4* mutant.
517 The $NO_2$-enhanced early callose formation upon elicitor treatment was strongly diminished in
518 the camalexin-deficient *pad3* mutant and in the *cyp79b2/b3* double mutant but was
519 unaffected in the indole glucosinolate mutant *cyp81f2* (Fig 11C,D). Only in the *cyp79b2/b3*
520 double mutant no chitosan-triggered callose depositions could be detected by microscopy
521 (Fig 11D). In many experiments, $NO_2$ alone already stimulated weak callose deposition,
522 which was also seen in the tested mutants except for *sid2* and *cyp79b2/b3*.
523

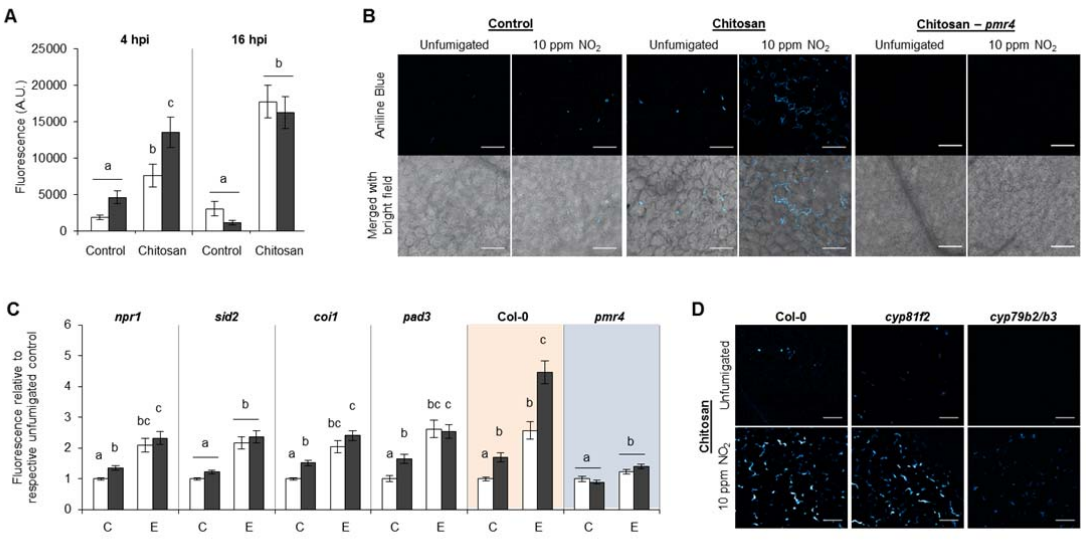


**Figure 11.** $NO_2$ pretreatment enhances early callose deposition upon treatment with the fungal elicitor chitosan. Plants were fumigated with 10 ppm $NO_2$ for 1 h and infiltrated with 500 µg/ml chitosan (0.04 % acetic acid as control) 4 h after fumigation. Leaf discs were obtained for callose quantification with Aniline Blue 4 h or 16 h after chitosan treatment. A, Callose quantification in Col-0. Columns represent means ± SEM; n = 34-44 from 10 plants per time point and treatment. B, Detection of Aniline blue-stained callose by confocal laser scanning microscopy. Fluorescence and bright field channels were merged using ImageJ software. Representative photographs were taken of $NO_2$-fumigated or unfumigated Col-0 or of *pmr4* (right panel) 4 h after treatment with chitosan. Scale = 100 µm. C, Callose quantification in mutants impaired in SA synthesis (*sid2*), SA signaling (*npr1*), JA signaling (*coi1*), camalexin synthesis (*pad3*), and callose deposition (*pmr4*). Columns represent means ± SE; n = 103-159 for Col-0 and *pmr4*, n = 57-65 for other mutants; white columns, unfumigated; black columns, 10 ppm $NO_2$. Letters indicate significant differences of all pairwise comparisons within time points via Kruskal Wallis Test plus Dunn`s post-hoc Test ($p < 0.05$). A.U., arbitrary unit; hpi, hours after infection; C, infiltration control; E, elicitor chitosan; white columns, unfumigated; black columns, 10 ppm $NO_2$. D, Detection of Aniline blue-stained callose in $NO_2$-fumigated or unfumigated *cyp81f2* and *cyp79b2/b3* mutant plants 4 h after treatment with chitosan. Col-0 stained in the same experiment is shown for comparison. Scale = 100 µm.

Two lines of evidence support an important role of callose in $NO_2$-induced pathogen resistance. (1.) The resistance was suppressed in the callose-deficient *pmr4* mutant and in plants treated with the callose inhibitor 2-DGG. (2.) Mutants that did not exhibit $NO_2$-induced resistance were also impaired in $NO_2$-enhanced callose deposition upon chitosan elicitation with the exception of *sid2*, which exhibited $NO_2$-induced pathogen immunity but impaired callose formation.

## DISCUSSION

Under physiological conditions $NO_2$ can arise from the oxidation of NO, reduction of nitrite, or decomposition of peroxynitrite (Pryor, 2006; Groß et al., 2013). Although the formation of $NO_2$ under stress conditions is well supported by direct and indirect evidence, less is known about physiological functions of $NO_2$. To address this issue, we fumigated Arabidopsis plants with ppm levels of $NO_2$ as a donor treatment. Previous experiments showed that one hour exposure of Arabidopsis to 30 ppm $NO_2$ triggered rapid cell death whereas 10 ppm $NO_2$ did not cause visible leaf symptoms or ion leakage as a marker of cell damage (Kasten et al., 2016). However, immediately after $NO_2$ exposure plants displayed enhanced chlorophyll autofluorescence (Fig.1 A, Supplemental Fig. S1) indicative of photoprotective energy dissipation in the course of a transient defense response (Lichtenthaler and Miehe, 1997; Chaerle and Van Der Straeten, 2000). In the current study the $NO_2$-induced defense response was investigated in detail.

Short-term exposure to 10 ppm $NO_2$ induced an up-regulation of more than 2300 genes immediately after the 1 h treatment period. The number of up-regulated genes decreased to approximately 750 at 6 h after fumigation, indicating that many genes were rapidly and transiently induced by $NO_2$ (Fig. 1 B,C). GO term enrichment and cluster analysis revealed that predominantly genes involved in pathogen resistance were strongly expressed after $NO_2$ fumigation (Fig. 2). Many of these genes are induced by flg22 (Zipfel et al., 2004), chitin (Ramonell et al., 2005), *B. cinerea* (Ferrari et al., 2007) and *P. syringae* (Lewis et al., 2015) (Fig. 2), suggesting that $NO_2$ triggered basal pathogen resistance or PTI.

Accordingly, $NO_2$ pre-treated plants showed resistance against the fungal pathogen *B. cinerea* and the bacterial pathogen *P. syringae* (Fig. 3). The fact that plants could fend off pathogens of distinct life styles confirmed that $NO_2$ conferred PTI. How the rather simple molecule $NO_2$ can specifically evoke pathogen resistance is not yet known. $NO_2$ might activate signaling cascades by nitration of electrophiles. Particularly, nitro-FAs such as nitro-linolenic acid have reported functions in defense and anti-inflammatory signaling (Schopfer et al., 2011; Mata-Pérez et al., 2016b). Alternatively, endogenous elicitors possibly derived from $NO_2$-induced cell wall- or membrane modifications are formed within the leaf. For instance, $NO_2$ can cause both oxidation as well as nitration of lipids (Pryor, 2006; Schopfer et al., 2011), which could lead to membrane damage and the subsequent formation of DAMPs. Such nitro signals and endogenous elicitors could also arise when $NO_2$ is formed under natural stress conditions.

568 Plant defense responses to pathogen assaults are often orchestrated by SA and JA,
569 although the exact interactions of these phytohormones in PTI are not fully understood
570 (Couto and Zipfel, 2016). SA levels increased 0-3 h after $NO_2$ fumigation, which was
571 accompanied by the increased expression of genes involved in the “early SA response” (Fig.
572 4, Supplemental Fig. S3) (Blanco et al., 2009) and SAR including *METHYL ESTERASE 9*
573 (*MES9*), *FLAVIN-DEPENDENT MONOOXYGENASE 1* (*FMO1*), *AZELAIC ACID INDUCED 1*
574 (*AZI1*), *AZI2*, *DEFECTIVE IN INDUCED RESISTANCE 1* (*DIR1*/*AZI6*), and AGD2-LIKE
575 *DEFENSE RESPONSE PROTEIN 1* (*ALD1*) (Supplemental Dataset S1). $NO_2$ also activated
576 the jasmonate biosynthesis pathway. The accumulation of OPDA 6 h after fumigation could
577 be responsible for the enhanced expression of 13 genes coding for antimicrobial defensins at
578 this time point (Figs. 5 and 6, Supplemental Dataset S1) as reported earlier (Stintzi et al.,
579 2001).
580
581 Notably, $NO_2$ did not only initiate jasmonate biosynthesis but also JA and JA-Ile catabolism
582 (Fig. 5). As a result, levels of JA and its bioactive derivate JA-Ile were unchanged whereas
583 their degradation products 12-OH-JA, 12-OH-JA-Ile, and 12-COOH-JA-Ile increased up to 3-
584 fold after fumigation (Figs. 5, 6). Several genes involved in jasmonate catabolism including
585 *JOX1-4* are inducible by jasmonates as a means of terminating the defense response
586 (Caarls et al., 2017; Smirnova et al., 2017). However, jasmonate-induced JA catabolism is
587 not a likely scenario after $NO_2$ exposure because neither JA nor JA-Ile levels were
588 significantly altered under these conditions. 12-OH-JA has reported functions in the down-
589 regulation of JA biosynthesis and JA-mediated defense responses (Miersch et al., 2008;
590 Patkar et al., 2015; Caarls et al., 2017; Smirnova et al., 2017) whereas biological activities of
591 other jasmonate hydroxylation and carboxylation products are yet unexplored. Genes coding
592 for proteins involved in SA/JA crosstalk such as several WRKY transcription factors,
593 GLUTAREDOXIN 480 (GRX480), UDP-DEPENDENT GLYCOSYLTRANSFERASE 76B1
594 (UGT76B1), and jasmonate-zim-domain (JAZ) transcriptional repressors were strongly up-
595 regulated (Supplemental Dataset S1) (von Saint Paul et al., 2011; Caarls et al., 2015).
596 Therefore, it is tempting to speculate that the $NO_2$-induced SA peak and proteins functioning
597 in SA/JA crosstalk control both the repression of JA-responsive genes as well as JA/JA-Ile
598 degradation, but this remains to be elucidated.
599
600 $NO_2$ fumigation triggered SA and OPDA signaling and defense gene expression. Further
601 experiments were aimed at detailing the role of phytohormones during the $NO_2$-induced
602 basal pathogen immunity. $NO_2$-induced *B. cinerea* resistance was compromised in plants
603 expressing the SA hydrolase NahG and in the SA signaling mutant *npr1* but was not altered
604 in the SA biosynthesis mutant *sid2* (Fig. 7). These results are in accordance with previous

findings, showing that SA produced by phenylalanine ammonia-lyase (PAL) but not the SID2 pathway contributes to the establishment of *B. cinerea* resistance in Arabidopsis (Ferrari et al., 2003). Further mutant analyses revealed that JA biosynthesis and signaling via the COI1 transcriptional activator was essential for $NO_2$-induced resistance against *Botrytis* as reported earlier (Thomma et al., 1998). Ethylene is well-known for its role in PTI (Boller and Felix, 2009; Couto and Zipfel, 2016). The GO term enrichment of genes involved in "ethylene-activated signaling pathways" indicated that that this gaseous defense hormone contributes to $NO_2$-induced immunity. However, this will need to be proven by future experiments.

The emission of the monoterpene α-pinene and the sesquiterpene longifolene were significantly increased after exposing plants to $NO_2$ (Fig. 8). It has been demonstrated that monoterpenes including α-pinene play an essential role in the SA-dependent establishment of SAR (Riedlmeier et al., 2017). Likewise, the transient $NO_2$-induced SA peak was followed by the emission of α-pinene, which might trigger SAR within and between plants as shown recently (Riedlmeier et al., 2017). α-Pinene production was not regulated on the transcriptional level because $NO_2$ exposure had no effect on the expression of *GGR1*, which codes for an enzyme involved in the biosynthesis of the monoterpene precursor geranyl diphosphate (Tholl and Lee, 2011) (Supplemental Dataset S1). $NO_2$-dependent increases of terpenoid emissions might originate from changes of metabolic pool size and fluxes (Ghirardo et al., 2014), and enzyme activities (Ghirardo et al., 2010). These results suggest the induction of local and systemic pathogen resistance by $NO_2$ analogous to the induction of a local PTI and subsequent establishment of SAR following the treatment with pathogen-derived elicitors (Mishina and Zeier, 2007).

Longifolene occurs commonly in plant species of the genus *Pinus,* where it is produced by longifolene synthases and stored in (oleo)resin (Martin et al., 2004). Treatment with methyl JA caused an enhanced accumulation of longifolene in Douglas-fir (*Pseudotsuga menziesii*) stem and root samples (Huber et al., 2005). In the resin longifolene could act as an antimicrobial compound (Himejima et al., 1992). Biosynthesis and functions of longifolene remain undocumented in Arabidopsis. However, it was reported that *CYP81D11*-overexpressing Arabidopsis lines emitted the sesquiterpene isolongifolene in the context of *cis*-jasmone-regulated tritrophic interactions between plants, aphids and parasitoids (Bruce et al., 2008). Noteworthy, *CYP81D11* was strongly induced by $NO_2$ (Supplemental Dataset S1).

641 The indole alkaloid camalexin and indole glucosinolates are both derived from tryptophan,
642 and their biosynthesis pathways are closely interconnected (Glawischnig et al., 2004). $NO_2$
643 fumigation triggered the expression of several genes involved in the production of these
644 compounds. *CYP79B2*, *CYP79B3*, *MYB51*, *CYP81F2*, and *PAD3* were further investigated
645 for their possible functions in $NO_2$-induced *B. cinerea* resistance because these genes have
646 been previously associated with immunity against fungal pathogens. The *cyp79b2/b3* mutant
647 is deficient in both camalexin as well as indole glucosinolates (Bednarek et al., 2009).
648 Experiments with this mutant confirmed the reported high susceptibility to *B. cinerea* (Nafisi
649 et al., 2007) and additionally revealed a complete loss of $NO_2$-induced resistance (Fig. 9 B).
650 Moreover, *myb51* plants, which have reduced levels of indolic compounds (Frerigmann et al.,
651 2016), were partially compromised in basal and $NO_2$-induced *B. cinerea* resistance.
652 Together, these results suggest an essential role of indolic secondary metabolites in $NO_2$-
653 induced *B. cinerea* immunity. *cyp81f2* mutant plants produce glucobrassicin but not 4-OH-
654 I3M and its derivatives, which are essential for basal resistance of Arabidopsis against
655 biotrophic powdery mildews and the necrotrophic fungal pathogen *Plectosphaerella*
656 *cucumerina* (Bednarek et al., 2009). However, in the current study *cyp81f2* plants did not
657 show a resistance-related phenotype indicating that CYP81F2-dependent indole
658 glucosinolates are dispensable for basal and $NO_2$-induced resistance against *B. cinerea* (Fig.
659 9 B).
660
661 Camalexin inhibits the growth of *B. cinerea* (Kliebenstein et al., 2005; Glawischnig, 2007).
662 $NO_2$ exposure triggered induction of the camalexin biosynthesis gene *PAD3*, and the *pad3*
663 mutant did not develop $NO_2$-induced resistance against *B. cinerea* (Fig. 9). Regarding the
664 compromised basal and $NO_2$-induced *B. cinerea* resistance, *pad3* had a similar phenotype to
665 the *cyp79b2/b3* mutant. Therefore, it was hypothesized that the *cyp79b2/b3* phenotype was
666 likely caused by camalexin deficiency rather than a defect in indole glucosinolate
667 biosynthesis. Unexpectedly, during *B. cinerea* infection neither *PAD3* expression nor
668 camalexin production were influenced by $NO_2$ pre-treatment. These findings resemble a
669 previous study showing that *PAD3* expression but not camalexin levels were strongly
670 increased upon elicitor treatment with plant cell wall-derived OGs (Ferrari et al., 2007). Thus,
671 rather than camalexin itself, a downstream metabolite (Bottcher et al., 2009) with so far
672 obscure physiological functions might be involved in $NO_2$-induced *B. cinerea* resistance.
673
674 In a pioneering attempt to identify such tryptophan-derived metabolites, we analyzed leaf
675 extracts from $NO_2$ treated plants using non-targeted direct infusion FT-ICR-MS. Nine
676 candidate metabolites significantly accumulated at 6 h after $NO_2$ fumigation but were not
677 detectable in leaf samples from *cyp79b2/b3* plants that are devoid of indolic compounds

(Supplemental Table S1). Five metabolites could represent indole derivatives because they contained at least 8 carbon and 1 nitrogen atom (Table 1). Neither camalexin nor known camalexin-related metabolites (Bottcher et al., 2009) were found among the $NO_2$-regulated CYP79B2/B3-dependent metabolites. Instead, measured exact masses were annotated as the indole glucosinolate glucobrassicin (I3M), its degradation product ascorbigen, and the methoxylated ascorbigen derivative 1,4-dimethoxyindol-3-ylmethylascorbate. If and how these candidate metabolites are linked to $NO_2$-induced *B. cinerea* resistance will be defined by future FT-ICR-MS runs with leaf extracts from air- and $NO_2$-exposed mutants including *pad3* and *cyp81f2*.

Cell wall fortification by callose deposition is a frequently used readout of PTI induction (Boller and Felix, 2009). In response to pathogens and pathogen-derived elicitors, callose is mostly synthesized by the callose synthase PMR4 (Jacobs et al., 2003; Nishimura et al., 2003; Clay et al., 2009; Ellinger and Voigt, 2014). $NO_2$-induced pathogen resistance was compromised in *pmr4* and in wild-type plants treated with a callose synthase inhibitor, implying a major role of callose in $NO_2$-induced *B. cinerea* immunity (Fig. 10). The fungal elicitor chitosan triggers callose formation (Kohle et al., 1985; Ramonell et al., 2005) and was used here to mimic the infection by a fungal pathogen. $NO_2$ alone already induced a slight increase in callose formation, which was further increased 4 h after chitosan application as compared to unfumigated plants (Fig. 11). Hence, preformed and more rapidly occurring callose deposition contributed to the $NO_2$-induced resistance against *B. cinerea*. The stimulatory effect of $NO_2$ on chitosan-induced callose formation was not seen in *npr1*, *sid2*, and *coi1*, indicating that SA and JA signaling were essential for induction of callose formation. However, given that the *sid2* mutant was capable of establishing $NO_2$-induced *B. cinerea* resistance (Fig. 7), this form of immunity is not solely based on callose depositions but can be compensated by other defense mechanisms.

It was reported that in Arabidopsis a yet uncharacterized CYP81F2- and PEN2-dependent 4-OH-I3M breakdown product functions as a signal or co-activator for Flg22-induced callose deposition (Clay et al., 2009). However, in the current study chitosan-triggered callose formation was not altered in *cyp81f2*, which is in line with the previous finding that Flg22- but not chitosan-triggered callose synthesis was affected in the *pen2* mutant (Luna et al., 2011). Hence, the regulation of callose build-up is specific to the perceived elicitor. Flg22-induced callose formation was not compromised in the *pad3* mutant suggesting that this defense response was not dependent on camalexin (Clay et al., 2009). Accordingly, Aniline blue fluorescence was significantly enhanced in *pad3* after chitosan treatment (Fig. 11 C). By contrast, the enhancing effect of $NO_2$ on the early chitosan-triggered callose deposition was

715 suppressed in *pad3* and *cyp79b2/b3* (Fig. 10 C,D). The latter mutant showed a reduced
716 ability to produce callose in response to chitosan, although this has to be confirmed by
717 quantitative measurements. Together, these findings argue for a role of PAD3-produced
718 metabolites other than camalexin in the $NO_2$-enhanced early callose deposition. The results
719 also suggest that chitosan-induced callose formation and the $NO_2$-enhanced callose
720 formation are controlled by different signaling pathways.
721
722 The lack of $NO_2$-enhanced callose formation 4 h after chitosan treatment in *pad3* and all
723 tested phytohormone mutants (except *sid2*) was associated with the inability of these
724 mutants to establish $NO_2$-induced *B. cinerea* resistance. Callose synthesis in response to
725 $NO_2$ alone was not altered in most of the tested mutants suggesting that only the $NO_2$-
726 enhanced callose formation upon perception of pathogen-derived elicitors was decisive for
727 the $NO_2$-induced immunity against *B. cinerea*.
728
729 **Summary**
730 Donor treatments of Arabidopsis with 10 ppm $NO_2$ triggered basal disease resistance against
731 *B. cinerea* and *P. syringae*. Transcriptomics suggested that $NO_2$ fumigation led to the onset
732 of phytohormone signaling and the biosynthesis of the indolic compounds such as
733 camalexin. Therefore, these biological processes were investigated in more detail. The $NO_2$-
734 induced resistance was dependent on SA and jasmonate signaling. An early peak of SA
735 immediately after the $NO_2$ treatment was followed by the transient accumulation of OPDA
736 and JA catabolites. Particularly interesting was the finding that activation of the JA
737 catabolism represents a mechanism for the complete suppression of JA signaling,
738 presumably in the course of SA/JA antagonism. Mutants impaired in SA or jasmonate
739 signaling were compromised in $NO_2$-induced *B. cinerea* resistance confirming that the
740 coordinate action of both signaling pathways is required for this form of pathogen immunity.
741
742 The *cyp79b2/b3* double mutant that is deficient in indole phytoalexins did not establish $NO_2$-
743 induced *B. cinerea* resistance. Further investigations of the *pad3* mutant combined with
744 biochemical measurements specified that unknown camalexin-derived metabolites but not
745 camalexin itself function in the resistance induction by $NO_2$. The SA and jasmonate signaling
746 mutants as well as the camalexin-deficient mutants were all more susceptible to *B. cinerea*
747 suggesting that basal resistance in untreated plants and $NO_2$-induced resistance are likely
748 mediated by similar defense mechanisms. The inability of these mutants to establish $NO_2$-
749 induced immunity was associated with loss of $NO_2$-enhanced callose formation upon
750 perception of the fungal elicitor chitosan. Therefore, timely callose deposition seems to be an
751 essential defense mechanism during the $NO_2$-induced *B. cinerea* resistance. Further defense

752 mechanisms could be related to the observed emission of α-pinene and longifolene from
753 $NO_2$-fumigated plants.
754
755 The exact mechanism by which $NO_2$ triggers PTI remains to be investigated. $NO_2$ might
756 function as a dedicated signal e.g. via nitration of electrophilic target molecules. However,
757 $NO_2$ could also act more indirectly as a defense elicitor by causing nitro-oxidative stress.
758
759 **MATERIALS AND METHODS**
760 **Plant material and $NO_2$ fumigation**
761 The utilized Arabidopsis (*Arabidopsis thaliana*) genotypes and their description and origin are
762 summarized in Supplemental Table S2. Plants were grown and fumigated for 1 h with 10
763 ppm $NO_2$ as described previously (Kasten et al., 2016). A fumigation system was used as
764 detailed in Supplemental Fig. S8 (Kasten et al., 2017). The only difference was the
765 installation of a $NO_2$ mixing cylinder (1.5 liter) containing Raschig rings, in which 15% NO
766 reacted with 100% $O_2$ to give $NO_2$. Up to 100 plants were fumigated with $NO_2$ in parallel. The
767 light conditions within the fumigation chamber were adjusted to the settings in the growth
768 chamber (65–85 µmol $m^{-2}$ $s^{-1}$ light intensity) where the plants were raised to avoid any light
769 artifacts on nitrogen metabolism (Beevers and Hageman, 1969) and plant-pathogen
770 interactions (Roden and Ingle, 2009).
771
772 **Autofluorescence detection**
773 UV-autofluorescence was detected using a hand-held UV lamp (Blak-Ray B-100AP; UVP)
774 and documented with a Nikon DC300 (Nikon). Camera settings were consistently kept at an
775 exposure time of 2 s at ISO-3200 with an aperture of F/18.
776
777 **Statistics**
778 SigmaPlot 12.0 (Systat Software Inc.) was used for the statistical evaluation of all data sets
779 as described earlier (Kasten et al., 2016). When comparing two independent groups, the
780 Student's *t*-test was used, in cases where the Shapiro-Wilk normality test ($p > 0.05$) was
781 passed. If the normality test failed, the analysis was done with the non-parametric Mann-
782 Whitney rank Sum Test. The comparison of more than two independent groups that passed
783 the Shapiro-Wilk normality test ($p > 0.05$) was done by One-Way ANOVA and subsequent
784 Holm-Sidak post-hoc tests for all pairwise comparisons or comparisons against a control
785 group. When the normality assumption of ANOVA failed on original or log-transformed data
786 (Shapiro-Wilk test), the non-parametric Kruskal-Wallis test with subsequent Dunn's Method
787 post-hoc test was performed to test for differences between the groups.
788

### ***Pseudomonas syringae* pv. *tomato* DC3000**

*Pseudomonas syringae* pv. *tomato* (*Pst*) DC3000 was cultivated at 28 °C for two days on selective NYGA agar (0.5% (w/v) bactoprotease pepton, 0.3% (w/v) yeast extract, 2% (v/v) glycerol, 1.8% (w/v) agar) supplemented with rifampicin and kanamycin (50 µg/ml). Five-week-old plants were fumigated with 10 ppm $NO_2$ (unfumigated plants as control) and inoculated 4 h after fumigation with 1 x $10^5$ colony-forming units per ml (cfu/ml) *Pst* DC3000 in 10 mM $MgCl_2$. Three to four leaves per plant were infiltrated with the bacterial suspension from their abaxial side using a 1 ml needle-less syringe. The *Pst* DC3000 bacterial titer within the leaves was determined 2 h (bacterial load control) or 1 and 2 days after infection. At the indicated time points 6-mm leaf discs were obtained from each infected leaf and, at the 2 h time point, surface sterilized for 30 s in 80% ethanol. Three leaf discs from different plants were merged into one biological replicate, which was then homogenized for 20 s in 200 µl 10 mM $MgCl_2$ using a Silamat S6 Tissue Homogenizer (Ivoclar Vivadent) and 1.7-2.0 mm glass beads. The resulting bacterial suspension was diluted in 10 mM $MgCl_2$ in a serial logarithmic dilution (10-fold) ranging from $10^0$ to $10^5$. Subsequently, 20 µl of each dilution was spotted onto selective nutrient-yeast extract glycerol (NYGA) agar before incubating them for two days at 28 °C. Bacterial colonies were counted in spots containing between 10 and 100 colonies and the bacterial titer (cfu/$cm^2$) per biological replicate was calculated as follows: cfu/$cm^2$ = colony count * dilution factor * Vol. total/Vol. spotted * 1.18 $cm^{-1}$ (leaf disc factor).

### ***Botrytis cinerea***

*B. cinerea* (strain SAS 56) was cultivated on halves of canned apricots (*Prunus armeniaca*) which were soaked for several hours in $ddH_2O$ to reduce their sugar content. After cultivating *B. cinerea* on the apricots for approximately one week, the spores were used for infection experiments. Leaves of four-week-old Arabidopsis plants were harvested 6 h after fumigation with 10 ppm $NO_2$ and placed with their abaxial side down onto 0.8% agar. Droplets (max. 10 µl) containing max 1000 spores of *B. cinerea* in half-strength grape juice were spotted onto the leaves, avoiding the middle vein. After a three-day incubation in a long-day climate chamber, the necrotic lesions were documented with a camera and their areas were determined via ImageJ 1.49m. The areas of the necrotic lesions developed on fumigated leaves were normalized to those formed on unfumigated leaves. $NO_2$-treated and untreated wild-type plants were always included during the evaluation of mutants. For the phytohormone, camalexine and RT-qPCR analyses, entire plants were infected with *B. cinerea* 6 h after fumigation with 10 ppm $NO_2$ (controls as indicated) by spraying a half-strength grape juice suspension containing 2 x $10^5$ fungal spores/ml and 0.01% Silwet L-77 (Lehle Seeds) onto the plants until run-off. The negative spray control contained no fungal

825 spores. The infected plants were covered with a clear lid to ensure high humidity for proper
826 infection.
827
828 **Phytohormone measurements**
829 To quantify SA, JA, *cis*-OPDA, OH-JA, OH-JA-Ile, and COOH-JA-Ile, approx. 250 mg leaf
830 material of four-week-old Col-0 plants that were fumigated with 10 ppm $NO_2$ or air was
831 harvested 0, 3, 6, and 24 h after fumigation. Similarly, leaf material from plants that were
832 spray-infected with *B. cinerea* 6 h after fumigation was collected 16, 24, and 48 h after
833 infection. The LC-MS/MS analyses were performed as described previously (Kasten et al.,
834 2016; Vadassery *et al.*, 2012).
835
836 **Camalexin measurements**
837 Four-week-old Col-0 plants were fumigated with 10 ppm $NO_2$ or air, and approximately 100
838 mg leaf material was collected and frozen in liquid nitrogen 6 h after fumigation. At the same
839 time, the remaining plants were spray-infected with *B. cinerea* and harvested 24 and 48 h
840 after infection as described above. Camalexin extraction and quantification was performed as
841 described previously (Frerigmann et al., 2015; Müller et al., 2015).
842
843 **FT-ICR-MS**
844 Four hundred fifty mg leaf material was frozen in liquid nitrogen, homogenized using a
845 Silamat S6 tissue homogenizer (Ivoclar Vivadent) and 1.7-2.0 mm glass pearls, and
846 subsequently incubated in 1.5 ml extraction buffer (2% acetic acid/80% ethanol) for 30 min at
847 4°C. After centrifugation for 20 min at 15,000 g and 4°C, the supernatant was collected and
848 the pellet was extracted again with 1.5 ml extraction buffer. An Oasis WAX 6cc solid phase
849 extraction (SPE) column (Waters) was rinsed with 1 ml methanol and 1 ml $H_2O$ before
850 addition of the 3 ml pooled leaf extract. The column was then washed with 2 ml 2% acetic
851 acid. Metabolites were recovered from the SPE columns by consecutive elutions with 2 ml
852 methanol and 2 ml 5% $NH_4OH$ in methanol. Samples were dried under vacuum, dissolved in
853 1 ml 70% methanol, centrifugated, and 200-fold diluted in 70% methanol before the MS run.
854
855 A Solarix FT-ICR mass spectrometer (Bruker Daltonics, Bremen, Germany) coupled to a 12
856 Tesla magnet (Magnex, UK) with an Infinity ICR cell was used for the experimental study. A
857 time domain transient was obtained with 4M Words size (4 million 32-integers) and was
858 Fourier transformed to obtain a frequency spectrum, which was then converted by the Solarix
859 Control program (Bruker Daltonics, Bremen, Germany) into a mass spectrum. All ion
860 excitations were performed in broadband mode (frequency sweep radial ion excitation).
861 Three hundred scans were accumulated for each mass spectrum. Ions were accumulated in

the collision cell for 300 ms for thermalization und enrichment prior to ICR ion detection. The base pressure in the ICR vacuum chamber was $7x10^{-10}$ mbar. The electrospray ionization source (Apollo II, Bruker Daltonics, Bremen, Germany) was used in the negative ionization mode to ionize the studied analytes in 70% methanolic solution (Lichrosolv, Sigma-Aldrich, Schnelldorf, Germany). The sample solutions were injected directly to the ionization source by the use of a microliter pump at a flow rate of 2 µL/min. A source heater temperature of 200 °C was maintained and no nozzle – skimmer fragmentation was performed in the ionization source. The instrument was previously calibrated by the use of Arginine negative cluster ions starting from a methanolic arginine solution of 5 mg/L.

Results of the FT-ICR-MS runs were subjected to normalization. Wilcoxon rank sum tests for differential analysis between samples from $NO_2$-fumigated plants and samples from air-fumigated plants were performed in R (version 3.3.3) using wilcox.test (R Core Team, 2014). Accurate masses corresponding to regulated metabolites were searched against public databases with Metlin (Smith et al., 2005) and MassTRIX (Suhre and Schmitt-Kopplin, 2008).

**Chitosan elicitation and callose quantification**

Four to five-week-old plants were treated with the fungal elicitor chitosan (medium molecular weight, Sigma-Aldrich) 4 h after they were fumigated with 10 ppm $NO_2$ (unfumigated plants as control). Here, three to four leaves per plant were infiltrated from their abaxial side with 500 µg/ml chitosan in 0.04% acetic acid using a 1 ml needle-less syringe. As a negative control, plants were treated with 0.04% acetic acid.

Leaf discs (6 mm) were obtained from treated leaves with a cork borer at the indicated time points and incubated overnight in 96% ethanol to remove chlorophyll. The destained leaf discs were gently dried off and then incubated for 1 h in 150 mM $K_2HPO_4$ buffer (pH 9.5) at room temperature (RT) and with mild agitation. Meanwhile, an Aniline Blue (Sigma-Aldrich) staining solution (0.01% (w/v) Aniline Blue in 150 m$MK_2HPO_4$ buffer, pH 9.5) was prepared and stirred until decolorized while protecting it from light. The samples were stained overnight in the dark at RT and with gentle agitation. After rinsing the leaf discs in the $K_2HPO_4$ buffer, they were transferred into wells of a black flat-bottom 96-well plate containing 50 µl of the same buffer. Callose was quantified by measuring the Aniline Blue fluorescence (mean of nine reads per leaf disc) with the Infinite M1000 Pro plate reader (Tecan) after adjusting the Z-positioning of the fluorescence top optics. Aniline Blue fluorescence was excited with 405 nm (5 nm bandwidth) and the emission wavelength was set to 490 nm (20 nm bandwidth). To minimize noise of potential autofluorescence, the fluorescence of leaf

discs which were incubated overnight in 150 mM $K_2HPO_4$ buffer (pH 9.5) without Aniline Blue was subtracted from the values of stained samples for each treatment.

For microscopic inspection of callose depositions, Aniline Blue-stained leaf discs were mounted in 50% glycerol and analyzed with the TCS SP8 X confocal laser scanning microscope (Leica) using the HC PL APO CS2 20x/0.75 IMM objective. The samples were excited with a Diode 405 Laser (Laser line UV 405 nm) at 0.1% laser intensity. The emitted fluorescence was detected with a photomultiplier (PMT) at 480 – 500 nm (gain 800), whereas bright field micrographs were taken at gain 400 using the Transmission PMT.

In some experiments leaves of four-week-old Col-0 plants were syringe-infiltrated with 1.2 mM of the callose synthesis inhibitor 2-deoxy-D-glucose (2-DDG, Sigma-Aldrich) or $ddH_2O$ 24 h before fumigation with 10 ppm $NO_2$ (unfumigated as control). Six hours after fumigation the infiltrated leaves were detached, placed on 0.8% agar, droplet-infected with *B. cinerea* and the necrotic lesions were analyzed after three days. The necrotic areas were compared to the ones formed on unfumigated and non-infiltrated leaves (= 100%).

**VOC collection and analysis**

Three to 4 biological replicates were collected in each of the 3 independent experiments ($n_{total}$ = 10-12). For each replicate, 50 Arabidopsis plants were enclosed in glass cuvettes continuously flushed with 200 ml $min^{-1}$ VOC-free synthetic air containing 400 ppm $CO_2$ and ~9000 ppm $H_2O$. The dynamic cuvette system and the experimental procedure has been previously described in detail (Riedlmeier et al., 2017). Sample collection was 8 h at 60 ml $min^{-1}$. To ensure collection of plant volatiles under steady-state conditions of net assimilation (Ghirardo et al., 2014), sampling started 1 h after plants were exposed to $NO_2$, and 2 h after the light was switched on in the morning for the days following the $NO_2$ fumigation. An overflow of ~140 ml $min^{-1}$ was maintained during the VOC collection to avoid any contaminations. Background measurements were performed for $NO_2$ and control samples separately, in exactly the same way as collections of samples, but plants were removed immediately after $NO_2$ or air fumigation for the treated and control plants, respectively. Quantitative and qualitative analysis of VOCs were achieved by thermal desorption-gas chromatography-mass spectrometry (TD-GC-MS) analysis following established methods (Ghirardo et al., 2011; Ghirardo et al., 2012; Ghirardo et al., 2016; Weikl et al., 2016). Breaking of VOCs through the polydimethylsiloxane (PDMS) adsorbent were negligible (0.08 ± 0.06%, sd, n = 8) at ~10 ppb of a 11-VOC standard mixture containing α-pinene (Apel-Riemer Environmental Inc). Longifolene was quantified using isolongifolene as pure standard. Fluxes of plant volatiles were calculated after background correction and

normalized to biomass dried weight (dw) of leaves. Successively, dw was converted in leaf area (la) by using the factor of 26.6 g $m^{-2}$ (dw $la^{-1}$), calculated from previous experiments (Riedlmeier et al., 2017).

**Microarray analysis**

Four-week-old Arabidopsis Col-0 plants were fumigated with 10 ppm $NO_2$ or air. Approximately 50 mg of pooled leaf material sampled from at least 2 different plants was harvested immediately and 6 h after fumigation and frozen in liquid nitrogen. Four biological replicates per treatment were collected. The samples were homogenized twice for 10 s using a Silamat S6 Tissue Homogenizer (Ivoclar Vivadent) and 1.7-2.0 mm glass beads. RNA was extracted and any potentially remaining DNA was digested using the RNeasy® Plant Mini Kit (Qiagen) according to the manufacturer's protocol. The gene expression measurements were performed using Agilent one-color microarrays as described recently (Riedlmeier et al., 2017). The Agilent Feature Extraction software was used with the template GE1_1100_Jul11. Gene expression levels were determined by the limma software (version 3.18.13) (Smyth, 2005) using the TAIR10 genome annotation (Berardini et al., 2015).The differential expression between $NO_2$ and air treatments for each timepoint was computed using the limma software (version 3.18.13) with a nested interaction model (Ritchie et al., 2015). Genes with adjusted *p*-values < 0.05 (based on the false discovery rate method for adjustment) and absolute $\log_2$ fold changes > 1 were selected for further analysis. The differential expression results were visualized via volcano plots generated by SigmaPlot 12.0 (Systat Software Inc.) and Venn diagrams created with jvenn (Bardou et al., 2014). Differentially expressed genes were subjected to GO-Term overrepresentation analysis with PANTHER 11.0 (release date: 2016-07-15) using the annotation from the Gene Ontology database (release date: 2016-12-28) and the Arabidopsis reference list from PANTHER (Mi et al., 2016). The obtained enriched GO terms ($p < 0.05$) were visualized in semantic similarity-based scatterplots generated with the REVIGO tool (Supek et al., 2011).

For the meta-analysis of stress-related expression responses, raw data and sample annotation from five Arabidopsis experiments (accession numbers E-GEOD-5684, E-GEOD-6176, E-GEOD-2538, E-GEOD-17382 and E-MTAB-4867) were downloaded from the ArrayExpress database (http://www.ebi.ac.uk/arrayexpress; (Kolesnikov et al., 2015)). The abiotic stress dataset (E-MTAB-4867) was selected because it was measured with the same microarray platform as the $NO_2$ fumigation data (Agilent At8x60K one-color microarrays, design ID: 29132). The pathogen and pathogen elicitor datasets (E-GEOD-5684, E-GEOD-6176, E-GEOD-2538, E-GEOD-17382) were found by keyword search. Due to unavailability of Agilent one-color microarray measurements, Affymetrix ATH1-121501 datasets were

chosen for these conditions. The combined Affymetrix data were preprocessed using the R package affy (version 1.40.0; (Gautier et al., 2004)). The combined Agilent data were preprocessed as stated for the $NO_2$ dataset. Based on TAIR10 annotation (Berardini et al., 2015), average log2 gene expression levels were computed and subsequently centered for each experiment relative to the mean of its controls to focus on treatment responses (log fold changes relative to mean of controls). Principal component analysis across all expression response profiles was performed in R (version 3.0.3) using prcomp (R Core Team, 2014).

**RT-qPCR**

RNA was isolated from approximately 100 mg leaf material using the RNeasy® Plant Mini Kit (Qiagen, Hilden, Germany) according to the manufacturers' instructions. If necessary samples were subjected to the RNA Clean Up Protocol of the RNeasy® Mini Kit (Qiagen, Hilden, Germany). Reverse transcription of 1 µg total RNA to cDNA was performed using the QuantiTect® Reverse Transcription Kit (Qiagen) according to the manufacturers' instructions. cDNA was diluted 1:16 in $ddH_2O$ prior to RT-qPCR, which was performed using the SensiMix™ SYBR® Low-ROX Kit (Bioline) and the following primers: *S16*fwd TTTACGCCATCCGTCAGAGTAT, *S16*rev TCTGGTAACGAGAACGAGCAC, *PAD3*fwd TACTTGTTGAGATGGCATTGTTGAA, *PAD3*rev CTTCCTCCTGCTTCGCCAAT. The annealing temperature was 60°C for all primers.

**Accession numbers**

The microarray data have been deposited in the ArrayExpress database at EMBL-EBI (https://www.ebi.ac.uk/arrayexpress/experiments/E-MTAB-6522).

**SUPPLEMENTAL DATA**

**Supplemental Figure S1.** $NO_2$ fumigation does not cause visible leaf symptoms

**Supplemental Figure S2.** GO term enrichment analysis of genes regulated by 10 ppm $NO_2$.

**Supplemental Figure S3.** Venn diagram showing that the expression of early SA response genes is induced after $NO_2$ fumigation.

**Supplemental Figure S4.** *B. cinerea*-induced SA and jasmonate accumulation is not altered by $NO_2$ pretreatment.

**Supplemental Figure S5.** Overview of volatiles emitted from Arabidopsis following the fumigation experiment.

**Supplemental Figure S6.** Effect of $NO_2$ fumigation on the volatile emissions.

**Supplemental Figure S7.** $NO_2$ treatment does not alter camalexin levels.

**Supplemental Figure S8.** The $NO_2$ fumigation system.

**Supplemental Dataset S1.** Microarray analysis of gene expression after fumigation of Arabidopsis for 1 h with 10 ppm $NO_2$.

**Supplemental Table S1.** Candidate tryptophan-derived metabolites involved in the plant response to $NO_2$.

**Supplemental Table S2.** Arabidopsis mutant lines used in this study.


## ACKNOWLEDGEMENTS

Erich Glawischnig was supported by a DFG Heisenberg Fellowship (GL346/5) and the TUM Junior Fellow Fund. We thank Michael Reichelt for support with the phytohormone measurements. Elisabeth Georgii was supported by the German Plant Phenotyping Network funded by the German Federal Ministry of Education and Research [DPPN, no. 031A053C]. We acknowledge the donation of *cyp81f2-2* mutant by Henning Frerigmann.


**Table I.** *CYP79B2/B3-dependent accumulation of metabolites 6 h after fumigation with 10 ppm $NO_2$*

Metabolites were not detected in the *cyp79b2/b3* double mutant. $NO_2$-induced up-regulation in wild-type plants is given as fold change of median spectral count. See Supplemental Table S1 for the complete data set including statistics. Formulae and tentative annotations were deduced from the exact masses as determined by Fourier transform ion cyclotron resonance mass spectrometry.

| Mass m/z $[M-H]^-$ | | Up-regulation by | Formula | Tentative annotation |
|---|---|---|---|---|
| Measured | Δ ppm | 10 ppm $NO_2$ | [M-H] | |
| 447.0537 | -0.05 | 1.8 | $C_{16}H_{20}N_2O_9S_2$ | Glucobrassicin, indol-3-ylmethylglucosinolate |
| 367.0783 | ±0.00 | 3.0 | $C_{15}H_{16}N_2O_9$ | Unknown *CYP79B2/B3*-dependent metabolite |
| 364.1038 | ±0.00 | 2.7 | $C_{17}H_{19}NO_8$ | 1,4-Dimethoxyindol-3-ylmethylascorbate |
| 304.0826 | -0.04 | 2.8 | $C_{15}H_{15}NO_6$ | Ascorbigen, indol-3-ylmethylascorbate |
| 232.0463 | ±0.00 | 2.2 | $C_8H_{11}NO_7$ | Unknown *CYP79B2/B3*-dependent metabolite |

## FIGURE LEGENDS

**Figure 1.** $NO_2$ triggers a rapid and transient defense response. Arabidopsis Col-0 plants were fumigated with 10 ppm $NO_2$ or air for 1 h. A, $NO_2$ caused no visible leaf damage (see also Supplemental Fig. S1) but a transient increase in red chlorophyll autofluorescence under UV light (white arrows) indicative of stress-induced photoprotective energy dissipation. B, Leaf material was harvested in quadruplicates for microarray analysis immediately or 6 h after fumigation. Volcano plots visualizing the changes in gene expression at 0 h and 6 h after fumigation by plotting the adjusted *p*-value over the fold change. Horizontal dashed lines mark $p = 0.05$; vertical dashed lines indicate $\log_2(FC) \pm 1$. Data points represent expression of individual genes. The expression of genes appearing in the colored left panels was significantly down-regulated ($p < 0.05$, $\log_2(FC) < -1$), whereas expression of genes within the colored right panels showed significant up-regulation ($p < 0.05$, $\log_2(FC) > 1$). C, Venn diagrams illustrating the number of genes that were significantly up- (top) or down-regulated (bottom) after $NO_2$ exposure with $p < 0.05$ and $\log_2(FC) \pm 1$. Color code is consistent in B and C indicating genes down-regulated immediately (grey), and 6 h (green) after fumigation or up-regulated immediately (blue) and 6 h (yellow) after fumigation.

**Figure 2.** $NO_2$–induced genes are related to pathogen defense. A, GO term enrichment of genes up-regulated directly (0 h) after fumigation. Enriched GO terms ($p < 0.05$) were identified using the PANTHER 11.0 overrepresentation test and visualized in scatter plots using the REVIGO tool. Each circle represents a GO term, and circle size represents the number of genes encompassed. The color code depicts the fold enrichment of the respective GO term within the data set compared to the PANTHER Arabidopsis reference list. Circles are clustered according to the distance of the respective GO terms within the GO hierarchical tree. Highly enriched or interesting GO terms were labeled. B, Principal component analysis of Arabidopsis gene expression responses to $NO_2$ fumigation, biotic stress, and abiotic stress. Data from microarray analysis after $NO_2$ fumigation were combined with previously published datasets representing responses to different stresses and elicitors (115 samples in total). The overall expression response similarities between samples of the combined dataset are visualized using the top two principal components (PCs), capturing 22% and 14% of the total variation, respectively. NO2, $NO_2$ fumigation; Bc, *Botrytis cinerea* infection, ArrayExpress accession number E-GEOD-5684; Ps, *Pseudomonas syringae* infection, E-GEOD-6176; Chitin, Chitin treatment, E-GEOD-2538; flg22, flagellin epitope 22 treatment, E-GEOD-17382; AS: abiotic stress treatment study, E-MTAB-4867; for each study, treated samples are marked by triangles and controls by circles.

**Figure 3.** $NO_2$ induces resistance against *B. cinerea* and *P. syringae*. A, Col-0 plants were fumigated or not (control) with 10 ppm $NO_2$ for 1 h, followed by droplet-infection of detached

leaves with approx. 1000 spores of *B. cinerea* 6 h after fumigation. Necrotic lesion area was measured 3 days later using ImageJ. Columns represent means of 18 independent experiments ± SE; n = 624-640. Asterisks indicate significant differences from control according to the Mann Whitney Rank Sum Test (***$p < 0.001$). Representative photographs of necrotic lesions 3 days after droplet-infection with *B. cinerea* are shown. Scale = 5 mm. B, Col-0 plants were fumigated with 10 ppm $NO_2$ for 1 h and syringe-infiltrated with $1x10^5$ cfu/ml *P. syringae* pv. *tomato* DC3000 4 h after fumigation. Leaf discs from infected leaves were obtained 2 hours or 1 and 2 days after infection to determine the bacterial titer (cfu/$cm^2$ leaf material). Columns represent means ± SE from 7 independent experiments; n (2 hpi) = 26-27, n (1 dpi) = 72, n (2 dpi) = 66. Asterisks indicate significant differences of all pairwise comparisons via Two Way ANOVA plus Holm-Sidak post-hoc Test (*$p < 0.05$, ***$p < 0.001$). hpi, hours post infection; dpi, days post infection; cfu, colony forming units; n.s., not significant; white columns, unfumigated; black columns, 10 ppm $NO_2$**.**

**Figure 4.** $NO_2$ induces signaling by SA. SA levels at different time points after fumigation with air or 10 ppm $NO_2$ were measured via LC-MS/MS and normalized to the samples' fresh weight (FW). Columns represent means ± SD; n = 5. Asterisks indicate significant differences within the time points as determined by Two Way ANOVA plus Holm-Sidak post-hoc Test (**$p < 0.01$,***$p < 0.001$). White columns, air; black columns: 10 ppm $NO_2$**.**

**Figure 5.** JA biosynthesis and degradation pathways are simultaneously up-regulated in response to $NO_2$. Schematic pathway of jasmonate metabolism illustrating the change in expression levels ($log_2$(FC)) of the respective genes obtained from the microarray analysis immediately (0 h, left part of colored panel) or 6 h (right part of colored panel) after fumigation with 10 ppm $NO_2$. Expression levels of all depicted genes can be found in Table S1. JA, jasmonic acid; OPDA, *cis*-(+)-12-oxophytodienoic acid; JA-Ile, jasmonoyl-L-isoleucine; MeJA, methyl jasmonate; 12-OH-JA, tuberonic acid; 12-OH-JA-Ile, hydroxyl-JA-Ile; 12-COOH-JA-Ile, dicarboxy-JA-Ile.

**Figure 6.** JA degradation products accumulate in response to $NO_2$. Various jasmonates were measured by LC-MS/MS at different time points after fumigation with air or 10 ppm $NO_2$. Concentrations were normalized to the leaf sample fresh weight (FW). A, OPDA, *cis*-(+)-12-oxophytodienoic acid; B, JA, jasmonic acid; C, JA-Ile, jasmonoyl-L-isoleucine; D, 12-OH-JA, tuberonic acid; E, 12-OH-JA-Ile; F, 12-COOH-JA-Ile. A-C, Products of JA biosynthesis pathway. D-F, JA catabolism products. Columns represent means ± SD; n = 5. Asterisks indicate significant differences within the time points according to Two Way ANOVA plus Holm-Sidak post-hoc Test (*$p < 0,05$, **$p < 0.01$,***$p < 0.001$). White columns, air; black

columns, 10 ppm $NO_2$.

**Figure 7.** SA and JA function in $NO_2$-induced resistance against *B. cinerea*. Mutants were subjected to *B. cinerea* droplet-infection 6 h after fumigation with 10 ppm $NO_2$ for 1 h. Necrotic areas were measured 3 days later and were normalized to the mean necrotic area of the respective unfumigated wild-type. A, SA-deficient (NahG, *sid2*) or SA-signaling (*npr1*) mutants and corresponding Col-0 wild-type. Columns represent means of at least 3 independent experiments ± SE; n = 95-331. B, JA-deficient *(aos, opr3*) or JA-signaling (*coi-1*) mutants and corresponding wild-types (Col-gl for *aos*, WS for *opr3*, Col-0 for *coi-1*). Columns represent means of three independent experiments ± SE; n = 66-126. Letters indicate significant differences of all pairwise comparisons via Kruskal Wallis Test plus Dunn`s post-hoc Test ($p < 0.05$). White columns, unfumigated; black columns, 10 ppm $NO_2$.

**Figure 8.** $NO_2$ exposure induces volatile emissions. A, Emission of the monoterpene α-pinene. B, Emission of the sesquiterpene longifolene. After 1 h of fumigation with 10 ppm $NO_2$, Arabidopsis Col-0 plants were enclosed in a flow-through cuvette system and volatile emissions were collected and successively analyzed by TD-GC-MS and multivariate data analysis (Supplemental Fig. S5, S6). Columns represent means ± SE; n = 10-12; Significant main effects ($NO_2$, Time) and interactions ($NO_2$ x Time) are shown (Two-Way ANOVA, all pairwise multiple comparison Holm-Sidak post-hoc test), *$p < 0.05$, **$p < 0.01$; n.d., not detected. White columns, control (air); black columns, 10 ppm $NO_2$.

**Figure 9.** $NO_2$-induced resistance against *B. cinerea* is dependent on *CYP79B2*, *CYP79B3*, and *PAD3* but independent of camalexin. A, The expression of genes related to the biosynthesis of tryptophan-derived indole glucosinolates and camalexin was strongly up-regulated after fumigation with 10 ppm $NO_2$ for 1 h. Colored panels indicate gene expression ($log_2$(FC)) immediately (left panel) or 6 h (right panel) after the $NO_2$ treatment. Genes that were investigated further are highlighted in bold letters. Gene regulation by transcription factors is indicated by dash line arrows. B, The *cyp79b2/b3* double mutant and the *myb51*, *cyp81f2*, and *pad3* mutants were subjected to *B. cinerea* droplet-infection 6 h after fumigation with 10 ppm $NO_2$ for 1 h. Necrotic areas were measured 3 days later and were normalized to the mean necrotic area of the unfumigated Col-0 wild-type. Columns represent means of three independent experiments ± SE; n = 81-418. Letters indicate significant differences of all pairwise comparisons via Kruskal Wallis Test plus Dunn`s post-hoc Test ($p < 0.01$). C, $NO_2$-exposed or control (unfumigated) Col-0 plants were spray-infected with 2 x $10^5$ *B. cinerea* spores 6 h after fumigation. *PAD3* transcript levels were quantified 16, 24, or 48 h after infection, relative to S16 expression via RT-qPCR. Columns represent means of two

1146 independent experiments ± SD; n = 5. Letters indicate significant differences of all pairwise
1147 comparisons within the time points via Two Way ANOVA plus Holm-Sidak post-hoc Test ($p$ <
1148 0.01). D, Plants were spray-infected with *B. cinerea* at 6 h after $NO_2$- or air-fumigation.
1149 Camalexin levels were measured by HPLC-MS 24 and 48 h after infection. Columns
1150 represent means ± SE; n = 12. Letters indicate significant differences of all pairwise
1151 comparisons within the time points via Two Way ANOVA plus Holm-Sidak post-hoc Test ($p$ <
1152 0.01).
1153
1154 **Figure 10.** Plants impaired in callose formation display a loss in $NO_2$-induced resistance
1155 against *B. cinerea.* A, Col-0 and callose-deficient *pmr4* plants were subjected to *B. cinerea*
1156 droplet-infection 6 h after fumigation with 10 ppm $NO_2$ for 1 h. Necrotic areas formed on
1157 fumigated leaves after 3 days were normalized to the mean necrotic area of the respective
1158 unfumigated leaves. Columns represent means of four independent experiments ± SE**;** n =
1159 135-145. B, Relative necrotic area determined on Col-0 plants that were infiltrated with 1.2
1160 mM of the callose-synthesis inhibitor 2-DDG ($H_2O$ as control) 24 h before fumigation followed
1161 by *B. cinerea* infection. Columns represent means ± SE**;** n = 70-130. (a, b) Letters indicate
1162 significant differences of all pairwise comparisons via Kruskal Wallis Test plus Dunn`s post-
1163 hoc Test ($p$ < 0.05). 2-DDG, 2-deoxy-D-glucose; white columns, unfumigated; black columns,
1164 10 ppm $NO_2$.
1165
1166 **Figure 11.** $NO_2$ pretreatment enhances early callose deposition upon treatment with the
1167 fungal elicitor chitosan*.* Plants were fumigated with 10 ppm $NO_2$ for 1 h and infiltrated with
1168 500 µg/ml chitosan (0.04 % acetic acid as control) 4 h after fumigation. Leaf discs were
1169 obtained for callose quantification with Aniline Blue 4 h or 16 h after chitosan treatment. A,
1170 Callose quantification in Col-0. Columns represent means ± SEM; n = 34-44 from 10 plants
1171 per time point and treatment. B, Detection of Aniline blue-stained callose by confocal laser
1172 scanning microscopy. Fluorescence and bright field channels were merged using ImageJ
1173 software. Representative photographs were taken of $NO_2$-fumigated or unfumigated Col-0 or
1174 of *pmr4* (right panel) 4 h after treatment with chitosan. Scale = 100 µm. C, Callose
1175 quantification in mutants impaired in SA synthesis (*sid2*), SA signaling (*npr1*), JA signaling
1176 (*coi1*), camalexin synthesis (*pad3*), and callose deposition (*pmr4*). Columns represent means
1177 ± SE; n = 103-159 for Col-0 and *pmr4,* n = 57-65 for other mutants; white columns,
1178 unfumigated; black columns, 10 ppm $NO_2$. Letters indicate significant differences of all
1179 pairwise comparisons within time points via Kruskal Wallis Test plus Dunn`s post-hoc Test ($p$
1180 < 0.05). A.U., arbitrary unit; hpi, hours after infection; C, infiltration control; E, elicitor
1181 chitosan; white columns, unfumigated; black columns, 10 ppm $NO_2$. D, Detection of Aniline
1182 blue-stained callose in $NO_2$-fumigated or unfumigated *cyp81f2* and *cyp79b2/b3* mutant plants

4 h after treatment with chitosan. Col-0 stained in the same experiment is shown for comparison. Scale = 100 μm.

## Parsed Citations


**Ahuja I, Kissen R, Bones AM (2012) Phytoalexins in defense against pathogens. Trends Plant Sci 17: 73–90**
Pubmed: Author and Title
Google Scholar: Author Only Title Only Author and Title

**Arasimowicz-Jelonek M, Floryszak-Wieczorek J (2011) Understanding the fate of peroxynitrite in plant cells - From physiology to pathophysiology. Phytochemistry 72: 681–688**
Pubmed: Author and Title
Google Scholar: Author Only Title Only Author and Title

**Bardou P, Mariette J, Escudié F, Djemiel C, Klopp C (2014) jvenn: an interactive Venn diagram viewer. BMC Bioinformatics 15: 293**
Pubmed: Author and Title
Google Scholar: Author Only Title Only Author and Title

**Bayles CJ, Ghemawat MS, Aist JR (1990) Inhibition by 2-deoxy-D-glucose of callose formation, papilla deposition, and resistance to powdery mildew in an ml-o barley mutant. Physiol Mol Plant Pathol 36: 63–72**
Pubmed: Author and Title
Google Scholar: Author Only Title Only Author and Title

**Bednarek P, Pislewska-Bednarek M, Svatos A, Schneider B, Doubsky J, Mansurova M, Humphry M, Consonni C, Panstruga R, Sanchez-Vallet A, et al (2009) A glucosinolate metabolism pathway in living plant cells mediates broad-spectrum antifungal defense. Science (80- ) 323: 101–106**
Pubmed: Author and Title
Google Scholar: Author Only Title Only Author and Title

**Beevers L, Hageman RH (1969) Nitrate reduction in higher plants. Annu Rev Plant Physiol 20: 495–522**
Pubmed: Author and Title
Google Scholar: Author Only Title Only Author and Title

**Berardini TZ, Reiser L, Li D, Mezheritsky Y, Muller R, Strait E, Huala E (2015) The arabidopsis information resource: Making and mining the "gold standard" annotated reference plant genome. Genesis 53: 474–485**
Pubmed: Author and Title
Google Scholar: Author Only Title Only Author and Title

**Bigeard J, Colcombet J, Hirt H (2015) Signaling mechanisms in pattern-triggered immunity (PTI). Mol Plant 8: 521–539**
Pubmed: Author and Title
Google Scholar: Author Only Title Only Author and Title

**Blanco F, Salinas P, Cecchini NM, Jordana X, Van Hummelen P, Alvarez ME, Holuigue L (2009) Early genomic responses to salicylic acid in Arabidopsis. Plant Mol Biol 70: 79–102**
Pubmed: Author and Title
Google Scholar: Author Only Title Only Author and Title

**Boller T, Felix G (2009) A renaissance of elicitors: perception of microbe-associated molecular patterns and danger signals by pattern-recognition receptors. Annu Rev Plant Biol 60: 379–406**
Pubmed: Author and Title
Google Scholar: Author Only Title Only Author and Title

**Bottcher C, Westphal L, Schmotz C, Prade E, Scheel D, Glawischnig E (2009) The Multifunctional Enzyme CYP71B15 (PHYTOALEXIN DEFICIENT3) Converts Cysteine-Indole-3-Acetonitrile to Camalexin in the Indole-3-Acetonitrile Metabolic Network of Arabidopsis thaliana. Plant Cell Online 21: 1830–1845**
Pubmed: Author and Title
Google Scholar: Author Only Title Only Author and Title

**Boudsocq M, Willmann MR, McCormack M, Lee H, Shan L, He P, Bush J, Cheng S-H, Sheen J (2010) Differential innate immune signalling via Ca2+ sensor protein kinases. Nature 464: 418–422**
Pubmed: Author and Title
Google Scholar: Author Only Title Only Author and Title

**Browse J (2009) Jasmonate passes muster: a receptor and targets for the defense hormone. Annu Rev Plant Biol 60: 183–205**
Pubmed: Author and Title
Google Scholar: Author Only Title Only Author and Title

**Bruce TJ a, Matthes MC, Chamberlain K, Woodcock CM, Mohib A, Webster B, Smart LE, Birkett M a, Pickett J a, Napier J a (2008) cis-Jasmone induces Arabidopsis genes that affect the chemical ecology of multitrophic interactions with aphids and their parasitoids. Proc Natl Acad Sci U S A 105: 4553–4558**
Pubmed: Author and Title
Google Scholar: Author Only Title Only Author and Title

**Caarls L, Elberse J, Awwanah M, Ludwig NR, de Vries M, Zeilmaker T, Van Wees SCM, Schuurink RC, Van den Ackerveken G (2017) Arabidopsis JASMONATE-INDUCED OXYGENASES down-regulate plant immunity by hydroxylation and inactivation of the hormone jasmonic acid. Proc Natl Acad Sci 114: 6388–6393**
Pubmed: Author and Title

Google Scholar: Author Only Title Only Author and Title

**Caarls L, Pieterse CMJ, Van Wees SCM (2015) How salicylic acid takes transcriptional control over jasmonic acid signaling. Front Plant Sci 6: 1–11**
Pubmed: Author and Title
Google Scholar: Author Only Title Only Author and Title

**Castillo M-C, Lozano-Juste J, Gonzalez-Guzman M, Rodriguez L, Rodriguez PL, Leon J (2015) Inactivation of PYR/PYL/RCAR ABA receptors by tyrosine nitration may enable rapid inhibition of ABA signaling by nitric oxide in plants. Sci Signal 8: ra89-ra89**
Pubmed: Author and Title
Google Scholar: Author Only Title Only Author and Title

**Chaerle L, Van Der Straeten D (2000) Imaging techniques and the early detection of plant stress. Trends Plant Sci 5: 495–501**
Pubmed: Author and Title
Google Scholar: Author Only Title Only Author and Title

**Clay NK, Adio AM, Denoux C, Jander G, Ausubel FM (2009) Glucosinolate Metabolites Required for an Arabidopsis Innate Immune Response. Science (80- ) 323: 95–101**
Pubmed: Author and Title
Google Scholar: Author Only Title Only Author and Title

**Corpas FJ, Barroso JB (2013) Nitro-oxidative stress vs oxidative or nitrosative stress in higher plants. New Phytol 199: 633–635**
Pubmed: Author and Title
Google Scholar: Author Only Title Only Author and Title

**Couto D, Zipfel C (2016) Regulation of pattern recognition receptor signalling in plants. Nat Rev Immunol 16: 537–552**
Pubmed: Author and Title
Google Scholar: Author Only Title Only Author and Title

**Delaney TP, Uknes S, Vernooij B, Friedrich L, Weymann K, Negrotto D, Gaffney T, Gut-rella M, Kessmann H, Ward E, et al (1994) A Central Role of Salicylic Acid in Plant Disease Resistance. 266: 1247–1250**
Pubmed: Author and Title
Google Scholar: Author Only Title Only Author and Title

**Ellinger D, Naumann M, Falter C, Zwikowics C, Jamrow T, Manisseri C, Somerville SC, Voigt CA (2013) Elevated Early Callose Deposition Results in Complete Penetration Resistance to Powdery Mildew in Arabidopsis. Plant Physiol 161: 1433–1444**
Pubmed: Author and Title
Google Scholar: Author Only Title Only Author and Title

**Ellinger D, Voigt CA (2014) Callose biosynthesis in arabidopsis with a focus on pathogen response: What we have learned within the last decade. Ann Bot 114: 1349–1358**
Pubmed: Author and Title
Google Scholar: Author Only Title Only Author and Title

**Ferrari S, Galletti R, Denoux C, De Lorenzo G, Ausubel FM, Dewdney J (2007) Resistance to Botrytis cinerea Induced in Arabidopsis by Elicitors Is Independent of Salicylic Acid, Ethylene, or Jasmonate Signaling But Requires PHYTOALEXIN DEFICIENT3. Plant Physiol 144: 367–379**
Pubmed: Author and Title
Google Scholar: Author Only Title Only Author and Title

**Ferrari S, Plotnikova JM, De Lorenzo G, Ausubel FM (2003) Arabidopsis local resistance to Botrytis cinerea involves salicylic acid and camalexin and requires EDS4 and PAD2, but not SID2, EDS5 or PAD4. Plant J 35: 193–205**
Pubmed: Author and Title
Google Scholar: Author Only Title Only Author and Title

**Frerigmann H, Glawischnig E, Gigolashvili T (2015) The role of MYB34, MYB51 and MYB122 in the regulation of camalexin biosynthesis in Arabidopsis thaliana. Front Plant Sci 6: 1–11**
Pubmed: Author and Title
Google Scholar: Author Only Title Only Author and Title

**Frerigmann H, Piślewska-Bednarek M, Sánchez-Vallet A, Molina A, Glawischnig E, Gigolashvili T, Bednarek P (2016) Regulation of Pathogen-Triggered Tryptophan Metabolism in Arabidopsis thaliana by MYB Transcription Factors and Indole Glucosinolate Conversion Products. Mol Plant 9: 682–695**
Pubmed: Author and Title
Google Scholar: Author Only Title Only Author and Title

**García-Andrade J, Ramírez V, Flors V, Vera P (2011) Arabidopsis ocp3 mutant reveals a mechanism linking ABA and JA to pathogen-induced callose deposition. Plant J 67: 783–794**
Pubmed: Author and Title
Google Scholar: Author Only Title Only Author and Title

**Gaupels F, Kuruthukulangarakoola GT, Durner J (2011) Upstream and downstream signals of nitric oxide in pathogen defence. Curr Opin Plant Biol 14: 707–714**
Pubmed: Author and Title
Google Scholar: Author Only Title Only Author and Title

**Gautier L, Cope L, Bolstad BM, Irizarry RA (2004) Affy - Analysis of Affymetrix GeneChip data at the probe level. Bioinformatics 20: 307–315**
Pubmed: Author and Title
Google Scholar: Author Only Title Only Author and Title

**Georgii E, Jin M, Zhao J, Kanawati B, Schmitt-Kopplin P, Albert A, Winkler JB, Schäffner AR (2017) Relationships between drought, heat and air humidity responses revealed by transcriptome-metabolome co-analysis. BMC Plant Biol 17: 120**
Pubmed: Author and Title
Google Scholar: Author Only Title Only Author and Title

**Ghirardo A, Gutknecht J, Zimmer I, Brüggemann N, Schnitzler JP (2011) Biogenic volatile organic compound and respiratory CO2 emissions after 13C-labeling: Online tracing of C translocation dynamics in poplar plants. PLoS One 6: 2–5**
Pubmed: Author and Title
Google Scholar: Author Only Title Only Author and Title

**Ghirardo A, Heller W, Fladung M, Schnitzler JP, Schroeder H (2012) Function of defensive volatiles in pedunculate oak (Quercus robur) is tricked by the moth Tortrix viridana. Plant, Cell Environ 35: 2192–2207**
Pubmed: Author and Title
Google Scholar: Author Only Title Only Author and Title

**Ghirardo A, Wright LP, Bi Z, Rosenkranz M, Pulido P, Rodriguez-Concepcion M, Niinemets U, Bruggemann N, Gershenzon J, Schnitzler J-P (2014) Metabolic Flux Analysis of Plastidic Isoprenoid Biosynthesis in Poplar Leaves Emitting and Nonemitting Isoprene. Plant Physiol 165: 37–51**
Pubmed: Author and Title
Google Scholar: Author Only Title Only Author and Title

**Ghirardo A, Xie J, Zheng X, Wang Y, Grote R, Block K, Wildt J, Mentel T, Kiendler-Scharr A, Hallquist M, et al (2016) Urban stress-induced biogenic VOC emissions and SOA-forming potentials in Beijing. Atmos Chem Phys 16: 2901–2920**
Pubmed: Author and Title
Google Scholar: Author Only Title Only Author and Title

**Glawischnig E (2007) Camalexin. Phytochemistry 68: 401–406**
Pubmed: Author and Title
Google Scholar: Author Only Title Only Author and Title

**Glawischnig E, Hansen BG, Olsen CE, Halkier BA (2004) Camalexin is synthesized from indole-3-acetaldoxime, a key branching point between primary and secondary metabolism in Arabidopsis. Proc Natl Acad Sci U S A 101: 8245–50**
Pubmed: Author and Title
Google Scholar: Author Only Title Only Author and Title

**Glazebrook J (2005) Contrasting Mechanisms of Defense Against Biotrophic and Necrotrophic Pathogens. Annu Rev Phytopathol 43: 205–227**
Pubmed: Author and Title
Google Scholar: Author Only Title Only Author and Title

**Groß F, Durner J, Gaupels F (2013) Nitric oxide, antioxidants and prooxidants in plant defence responses. Front Plant Sci 4: 419**
Pubmed: Author and Title
Google Scholar: Author Only Title Only Author and Title

**Heil M, Land WG (2014) Danger signals - damaged-self recognition across the tree of life. Front Plant Sci 5: 578**
Pubmed: Author and Title
Google Scholar: Author Only Title Only Author and Title

**Heitz T, Smirnova E, Widemann E, Aubert Y, Pinot F, Ménard R (2016) Lipids in Plant and Algae Development. doi: 10.1007/978-3-319-25979-6**
Pubmed: Author and Title
Google Scholar: Author Only Title Only Author and Title

**Heitz T, Widemann E, Lugan R, Miesch L, Ullmann P, Désaubry L, Holder E, Grausem B, Kandel S, Miesch M, et al (2012) Cytochromes P450 CYP94C1 and CYP94B3 catalyze two successive oxidation steps of plant hormone jasmonoyl-isoleucine for catabolic turnover. J Biol Chem 287: 6296–6306**
Pubmed: Author and Title
Google Scholar: Author Only Title Only Author and Title

**Himejima M, Hobson KR, Otsuka T, Wood DL, Kubo I (1992) Antimicrobial terpenes from oleoresin of ponderosa pine tree Pinus ponderosa: A defense mechanism against microbial invasion. J Chem Ecol 18: 1809–1818**
Pubmed: Author and Title
Google Scholar: Author Only Title Only Author and Title

**Huber DPW, Philippe RN, Madilao LL, Sturrock RN, Bohlmann J (2005) Changes in anatomy and terpene chemistry in roots of Douglas-fir seedlings following treatment with methyl jasmonate. Tree Physiol 25: 1075–1083**
Pubmed: Author and Title
Google Scholar: Author Only Title Only Author and Title

**Hull AK, Vij R, Celenza JL (2000) Arabidopsis cytochrome P450s that catalyze the first step of tryptophan-dependent indole-3-acetic acid biosynthesis. Proc Natl Acad Sci 97: 2379–2384**
Pubmed: Author and Title
Google Scholar: Author Only Title Only Author and Title

**Jacobs AK, Lipka V, Burton RA, Panstruga R, Strizhov N, Schulze-Lefert P, Fincher GB (2003) An Arabidopsis Callose Synthase, GSL5, Is Required for Wound and Papillary Callose Formation. Plant Cell 15: 2503–2513**
Pubmed: Author and Title
Google Scholar: Author Only Title Only Author and Title

**Joudoi T, Shichiri Y, Kamizono N, Akaike T, Sawa T, Yoshitake J, Yamada N, Iwai S (2013) Nitrated Cyclic GMP Modulates Guard Cell Signaling in Arabidopsis. Plant Cell 25: 558–571**
Pubmed: Author and Title
Google Scholar: Author Only Title Only Author and Title

**Kasten D, Durner J, Gaupels F (2017) Gas alert: The NO2 pitfall during NO fumigation of plants. Front Plant Sci 8: 8–11**
Pubmed: Author and Title
Google Scholar: Author Only Title Only Author and Title

**Kasten D, Mithöfer A, Georgii E, Lang H, Durner J, Gaupels F (2016) Nitrite is the driver, phytohormones are modulators while NO and H2O2 act as promoters of NO2-induced cell death. J Exp Bot 67: 6337–6349**
Pubmed: Author and Title
Google Scholar: Author Only Title Only Author and Title

**Kitaoka N, Matsubara T, Sato M, Takahashi K, Wakuta S, Kawaide H, Matsui H, Nabeta K, Matsuura H (2011) Arabidopsis CYP94B3 encodes jasmonyl-L-isoleucine 12-hydroxylase, a key enzyme in the oxidative catabolism of jasmonate. Plant Cell Physiol 52: 1757–1765**
Pubmed: Author and Title
Google Scholar: Author Only Title Only Author and Title

**Klepper L (1990) Comparison between NO(x) Evolution Mechanisms of Wild-Type and nr(1) Mutant Soybean Leaves. Plant Physiol 93: 26–32**
Pubmed: Author and Title
Google Scholar: Author Only Title Only Author and Title

**Klepper L (1979) Nitric oxide (NO) and nitrogen dioxide (NO2) emissions from herbicide-treated soybean plants. Atmos Environ 13: 537–542**
Pubmed: Author and Title
Google Scholar: Author Only Title Only Author and Title

**Kliebenstein DJ, Rowe HC, Denby KJ (2005) Secondary metabolites influence Arabidopsis/Botrytis interactions: Variation in host production and pathogen sensitivity. Plant J 44: 25–36**
Pubmed: Author and Title
Google Scholar: Author Only Title Only Author and Title

**Kohle H, Jeblick W, Poten F, Blaschek W, Kauss H (1985) Chitosan-Elicited Callose Synthesis in Soybean Cells as a. Plant Physiol 77: 544–551**
Pubmed: Author and Title
Google Scholar: Author Only Title Only Author and Title

**Kolbert Z, Feigl G, Bordé Á, Molnár Á, Erdei L (2017) Protein tyrosine nitration in plants: Present knowledge, computational prediction and future perspectives. Plant Physiol Biochem 113: 56–63**
Pubmed: Author and Title
Google Scholar: Author Only Title Only Author and Title

**Kolesnikov N, Hastings E, Keays M, Melnichuk O, Tang YA, Williams E, Dylag M, Kurbatova N, Brandizi M, Burdett T, et al (2015) ArrayExpress update-simplifying data submissions. Nucleic Acids Res 43: D1113–D1116**
Pubmed: Author and Title
Google Scholar: Author Only Title Only Author and Title

**Koo AJK, Cooke TF, Howe GA (2011) Cytochrome P450 CYP94B3 mediates catabolism and inactivation of the plant hormone jasmonoyl-L-isoleucine. Proc Natl Acad Sci 108: 9298–9303**
Pubmed: Author and Title
Google Scholar: Author Only Title Only Author and Title

**Lewis LA, Polanski K, de Torres-Zabala M, Jayaraman S, Bowden L, Moore J, Penfold CA, Jenkins DJ, Hill C, Baxter L, et al (2015) Transcriptional Dynamics Driving MAMP-Triggered Immunity and Pathogen Effector-Mediated Immunosuppression in Arabidopsis Leaves Following Infection with Pseudomonas syringae pv tomato DC3000. Plant Cell 27: 3038–3064**
Pubmed: Author and Title
Google Scholar: Author Only Title Only Author and Title

**Lichtenthaler H, Miehe J (1997) Fluorescence imaging as a diagnostic tool for plant stress. Trends Plant Sci 2: 6–10**
Pubmed: Author and Title
Google Scholar: Author Only Title Only Author and Title

**Liu X, Hou F, Li G, Sang N (2015) Effects of nitrogen dioxide and its acid mist on reactive oxygen species**

**production and antioxidant enzyme activity in Arabidopsis plants. J Environ Sci 34: 93–99**
Pubmed: Author and Title
Google Scholar: Author Only Title Only Author and Title

**Luna E, Pastor V, Robert J, Flors V, Mauch-Mani B, Ton J (2011) Callose deposition: a multifaceted plant defense response. Mol Plant-Microbe Interact 24: 183–193**
Pubmed: Author and Title
Google Scholar: Author Only Title Only Author and Title

**Maassen A, Hennig J (2011) Effect of Medicago sativa Mhb1 gene expression on defense response of Arabidopsis thaliana plants. Acta Biochim Pol 58: 427–432**
Pubmed: Author and Title
Google Scholar: Author Only Title Only Author and Title

**Martin DM, Fäldt J, Bohlmann J (2004) Functional Characterization of Nine Norway SpruceTPS Genes and Evolution of GymnospermTerpene Synthases of the TPS-d Subfamily. Plant Physiol 135: 1908–1927**
Pubmed: Author and Title
Google Scholar: Author Only Title Only Author and Title

**Mata-Pérez C, Begara-Morales JC, Chaki M, Sánchez-Calvo B, Valderrama R, Padilla MN, Corpas FJ, Barroso JB (2016a) Protein Tyrosine Nitration during Development and Abiotic Stress Response in Plants. Front Plant Sci 7: 1–7**
Pubmed: Author and Title
Google Scholar: Author Only Title Only Author and Title

**Mata-Pérez C, Sánchez-Calvo B, Padilla MN, Begara-Morales JC, Luque F, Melguizo M, Jiménez-Ruiz J, Fierro-Risco J, Peñas-Sanjuán A, Valderrama R, et al (2016b) Nitro-Fatty Acids in Plant Signaling: Nitro-Linolenic Acid Induces the Molecular Chaperone Network in Arabidopsis. Plant Physiol 170: 686–701**
Pubmed: Author and Title
Google Scholar: Author Only Title Only Author and Title

**Mengiste T (2012) Plant Immunity to Necrotrophs. Annu Rev Phytopathol 50: 267–294**
Pubmed: Author and Title
Google Scholar: Author Only Title Only Author and Title

**Mi H, Huang X, Muruganujan A, Tang H, Mills C, Kang D, Thomas PD (2016) PANTHER version 11: Expanded annotation data from Gene Ontology and Reactome pathways, and data analysis tool enhancements. Nucleic Acids Res 45: D183–D189**
Pubmed: Author and Title
Google Scholar: Author Only Title Only Author and Title

**Miersch O, Neumerkel J, Dippe M, Stenzel I, Wasternack C (2008) Hydroxylated jasmonates are commonly occurring metabolites of jasmonic acid and contribute to a partial switch-off in jasmonate signaling. New Phytol 177: 114–127**
Pubmed: Author and Title
Google Scholar: Author Only Title Only Author and Title

**Mishina TE, Zeier J (2007) Pathogen-associated molecular pattern recognition rather than development of tissue necrosis contributes to bacterial induction of systemic acquired resistance in Arabidopsis. Plant J 50: 500–513**
Pubmed: Author and Title
Google Scholar: Author Only Title Only Author and Title

**Müller TM, Böttcher C, Morbitzer R, Götz CC, Lehmann J, Lahaye T, Glawischnig E (2015) TRANSCRIPTION ACTIVATOR-LIKE EFFECTOR NUCLEASE-Mediated Generation and Metabolic Analysis of Camalexin-Deficient cyp71a12 cyp71a13 Double Knockout Lines. Plant Physiol 168: 849–858**
Pubmed: Author and Title
Google Scholar: Author Only Title Only Author and Title

**Mur LAJ, Mandon J, Persijn S, Cristescu SM, Moshkov IE, Novikova G V., Hall MA, Harren FJM, Hebelstrup KH, Gupta KJ (2013) Nitric oxide in plants: An assessment of the current state of knowledge. AoB Plants 5: 1–17**
Pubmed: Author and Title
Google Scholar: Author Only Title Only Author and Title

**Nafisi M, Goregaoker S, Botanga CJ, Glawischnig E, Olsen CE, Halkier BA, Glazebrook J (2007) Arabidopsis Cytochrome P450 Monooxygenase 71A13 Catalyzes the Conversion of Indole-3-Acetaldoxime in Camalexin Synthesis. Plant Cell 19: 2039–2052**
Pubmed: Author and Title
Google Scholar: Author Only Title Only Author and Title

**Nawrath C, Métraux JP (1999) Salicylic acid induction-deficient mutants of Arabidopsis express PR-2 and PR-5 and accumulate high levels of camalexin after pathogen inoculation. Plant Cell 11: 1393–404**
Pubmed: Author and Title
Google Scholar: Author Only Title Only Author and Title

**Niinemets Ü (2010) Mild versus severe stress and BVOCs: thresholds, priming and consequences. Trends Plant Sci 15: 145–153**
Pubmed: Author and Title
Google Scholar: Author Only Title Only Author and Title

**Nishimura MT, Stein M, Hou B-H, Vogel JP, Edwards H, Somerville SC (2003) Loss of a Callose Synthase Results in Salicylic Acid –**

**Dependent Disease resitance. Science (80- ) 301: 969–972**
Pubmed: Author and Title
Google Scholar: Author Only Title Only Author and Title

**Park JH, Halitschke R, Kim HB, Baldwin IT, Feldmann KA, Feyereisen R (2002) A knock-out mutation in allene oxide synthase results in male sterility and defective wound signal transduction in Arabidopsis due to a block in jasmonic acid biosynthesis. Plant J 31: 1–12**
Pubmed: Author and Title
Google Scholar: Author Only Title Only Author and Title

**Patkar RN, Benke PI, Qu Z, Constance Chen YY, Yang F, Swarup S, Naqvi NI (2015) A fungal monooxygenase-derived jasmonate attenuates host innate immunity. Nat Chem Biol 11: 733–740**
Pubmed: Author and Title
Google Scholar: Author Only Title Only Author and Title

**Pieterse CMJ, Van der Does D, Zamioudis C, Leon-Reyes A, Van Wees SCM (2012) Hormonal Modulation of Plant Immunity. Annu Rev Cell Dev Biol 28: 489–521**
Pubmed: Author and Title
Google Scholar: Author Only Title Only Author and Title

**Pryor WA (2006) Free radical biology and medicine: it's a gas, man! AJP Regul Integr Comp Physiol 291: R491–R511**

**R Core Team (2014) R: A language and environment for statistical computing. R Found. Stat. Comput. Vienna, Austria. http//www.r-project.org**
Pubmed: Author and Title
Google Scholar: Author Only Title Only Author and Title

**Radi R (2012) Protein Tyrosine Nitration: Biochemical Mechanisms and Structural Basis of Functional Effects. Acc Chem Res. doi: 10.1021/ar300234c**
Pubmed: Author and Title
Google Scholar: Author Only Title Only Author and Title

**Ramonell K, Berrocal-Lobo M, Koh S, Wan J, Edwards H, Stacey G, Somerville S (2005) Loss-of-function mutations in chitin responsive genes show increased susceptibility to the powdery mildew pathogen erysiphe cichoracearum. Plant Physiol 138: 1027–1036**
Pubmed: Author and Title
Google Scholar: Author Only Title Only Author and Title

**Rauhut T, Luberacki B, Seitz HU, Glawischnig E (2009) Inducible expression of a Nep1-like protein serves as a model trigger system of camalexin biosynthesis. Phytochemistry 70: 185–189**
Pubmed: Author and Title
Google Scholar: Author Only Title Only Author and Title

**Riedlmeier M, Ghirardo A, Wenig M, Knappe C, Koch K, Georgii E, Dey S, Parker JE, Schnitzler J-P, Vlot C (2017) Monoterpenes support systemic acquired resistance within and between plants. Plant Cell 29: tpc.00898.2016**
Pubmed: Author and Title
Google Scholar: Author Only Title Only Author and Title

**Ritchie ME, Phipson B, Wu D, Hu Y, Law CW, Shi W, Smyth GK (2015) limma powers differential expression analyses for RNA-sequencing and microarray studies. Nucleic Acids Res 43: e47**
Pubmed: Author and Title
Google Scholar: Author Only Title Only Author and Title

**Robert-Seilaniantz A, Grant M, Jones JDG (2011) Hormone Crosstalk in Plant Disease and Defense: More Than Just JASMONATE-SALICYLATE Antagonism. Annu Rev Phytopathol 49: 317–343**
Pubmed: Author and Title
Google Scholar: Author Only Title Only Author and Title

**Roden LC, Ingle RA (2009) Lights, Rhythms, Infection: The Role of Light and the Circadian Clock in Determining the Outcome of Plant-Pathogen Interactions. Plant Cell Online 21: 2546–2552**
Pubmed: Author and Title
Google Scholar: Author Only Title Only Author and Title

**Rogers EE, Glazebrook J, Ausubel FM (1996) Mode of action of the Arabidopsis thaliana phytoalexin camalexin and its role in Arabidopsis-pathogen interactions. Mol Plant Microbe Interact 9: 748–757**
Pubmed: Author and Title
Google Scholar: Author Only Title Only Author and Title

**von Saint Paul V, Zhang W, Kanawati B, Geist B, Faus-Keßler T, Schmitt-Kopplin P, Schäffner AR (2011) The Arabidopsis Glucosyltransferase UGT76B1 Conjugates Isoleucic Acid and Modulates Plant Defense and Senescence. Plant Cell 23: 4124–4145**
Pubmed: Author and Title
Google Scholar: Author Only Title Only Author and Title

**Sakamoto A, Sakurao SH, Fukunaga K, Matsubara T, Ueda-Hashimoto M, Tsukamoto S, Takahashi M, Morikawa H (2004) Three distinct Arabidopsis hemoglobins exhibit peroxidase-like activity and differentially mediate nitrite-dependent protein nitration. FEBS Lett 572: 27–32**
Pubmed: Author and Title

Google Scholar: Author Only Title Only Author and Title

**Sakihama Y, Tamaki R, Shimoji H, Ichiba T, Fukushi Y, Tahara S, Yamasaki H (2003) Enzymatic nitration of phytophenolics: Evidence for peroxynitrite- independent nitration of plant secondary metabolites. FEBS Lett 553: 377–380**
Pubmed: Author and Title
Google Scholar: Author Only Title Only Author and Title

**Schopfer FJ, Cipollina C, Freeman BA (2011) Formation and Signaling Actions of Electrophilic Fatty Acids. 5997–6021**
Pubmed: Author and Title
Google Scholar: Author Only Title Only Author and Title

**Schuhegger R, Nafisi M, Mansourova M, Petersen BL, Olsen CE, Svatos A, Halkier BA, Glawischnig E (2006) CYP71B15 (PAD3) catalyzes the final step in camalexin biosynthesis. Plant Physiol 141: 1248–1254**
Pubmed: Author and Title
Google Scholar: Author Only Title Only Author and Title

**Shibata H, Kono Y, Yamshita S, Sawa Y, Ochiai H, Tanaka K (1995) Degradation of chlorophyll by nitrogen dioxide generated from the peroxidase reaction. Biochim Biophys Acta 1230: 45–50**
Pubmed: Author and Title
Google Scholar: Author Only Title Only Author and Title

**Shimazaki KI, Yu SW, Sakaki T, Tanaka K (1992) Differences between spinach and kidney bean plants in terms of sensitivity to fumigation with NO2. Plant Cell Physiol 33: 267–252**
Pubmed: Author and Title
Google Scholar: Author Only Title Only Author and Title

**Smirnova E, Marquis V, Poirier L, Aubert Y, Zumsteg J, Ménard R, Miesch L, Heitz T (2017) Jasmonic Acid Oxidase 2 (JAO2) hydroxylates jasmonic acid and represses basal defense and resistance responses against Botrytis cinerea infection. Mol Plant 1159–1173**
Pubmed: Author and Title
Google Scholar: Author Only Title Only Author and Title

**Smith CA, O 'maille G, Want EJ, Qin C, Trauger SA, Brandon TR, Custodio DE, Abagyan R, Siuzdak G (2005) METLIN: a metabolite mass spectral database. Proc 9Th Int Congr Ther Drug Monit Clin Toxicol 27: 747–751**
Pubmed: Author and Title
Google Scholar: Author Only Title Only Author and Title

**Smyth GK (2005) Limma: linear models for microarray data BT - Bioinformatics and Computational Biology Solutions Using R and Bioconductor. Bioinforma Comput Biol Solut Using R Bioconductor. doi: 10.1007/0-387-29362-0_23**
Pubmed: Author and Title
Google Scholar: Author Only Title Only Author and Title

**Sparks JP (2009) Ecological ramifications of the direct foliar uptake of nitrogen. Oecologia 159: 1–13**
Pubmed: Author and Title
Google Scholar: Author Only Title Only Author and Title

**Srivastava HS, Ormrod DP, Hale BA (1994) Responses of greening bean seedling leaves to nitrogen dioxide and nutrient nitrate supply. Environ Polllution 86: 2–7**
Pubmed: Author and Title
Google Scholar: Author Only Title Only Author and Title

**Stintzi A, Browse J (2000) The Arabidopsis male-sterile mutant, opr3, lacks the 12-oxophytodienoic acid reductase required for jasmonate synthesis. Proc Natl Acad Sci U S A 97: 10625–10630**
Pubmed: Author and Title
Google Scholar: Author Only Title Only Author and Title

**Stintzi A, Weber H, Reymond P, Browse J, Farmer EE (2001) Plant defense in the absence of jasmonic acid: the role of cyclopentenones. Proc Natl Acad Sci U S A 98: 12837–42**
Pubmed: Author and Title
Google Scholar: Author Only Title Only Author and Title

**Suhre K, Schmitt-Kopplin P (2008) MassTRIX: mass translator into pathways. Nucleic Acids Res 36: 481–484**
Pubmed: Author and Title
Google Scholar: Author Only Title Only Author and Title

**Supek F, Bošnjak M, Škunca N, Šmuc T (2011) Revigo summarizes and visualizes long lists of gene ontology terms. PLoS One. doi: 10.1371/journal.pone.0021800**
Pubmed: Author and Title
Google Scholar: Author Only Title Only Author and Title

**Takahashi M, Furuhashi T, Ishikawa N, Horiguchi G, Sakamoto A, Tsukaya H, Morikawa H (2014) Nitrogen dioxide regulates organ growth by controlling cell proliferation and enlargement in Arabidopsis. New Phytol 201: 1304–1315**
Pubmed: Author and Title
Google Scholar: Author Only Title Only Author and Title

**Tholl D, Lee S (2011) Terpene spezialized metabolism in Arabidopsis thaliana. Arab B 25: 1075–1083**
Pubmed: Author and Title
Google Scholar: Author Only Title Only Author and Title

**Thomas DD, Ridnour LA, Isenberg JS, Flores-Santana W, Switzer CH, Donzelli S, Hussain P, Vecoli C, Paolocci N, Ambs S, et al (2008) The chemical biology of nitric oxide: Implications in cellular signaling. Free Radic Biol Med 45: 18–31**
Pubmed: Author and Title
Google Scholar: Author Only Title Only Author and Title

**Thomma BPHJ, Eggermont K, Penninckx IAMA, Mauch-Mani B, Vogelsang R, Cammue BPA, Broekaert WF (1998) Separate jasmonate-dependent and salicylate-dependent defense-response pathways in Arabidopsis are essential for resistance to distinct microbial pathogens. Proc Natl Acad Sci U S A 95: 15107–15111**
Pubmed: Author and Title
Google Scholar: Author Only Title Only Author and Title

**Vadassery J, Reichelt M, Hause B, Gershenzon J, Boland W, Mithofer a. (2012) CML42-Mediated Calcium Signaling Coordinates Responses to Spodoptera Herbivory and Abiotic Stresses in Arabidopsis. Plant Physiol 159: 1159–1175**
Pubmed: Author and Title
Google Scholar: Author Only Title Only Author and Title

**Vlot AC, Dempsey DA, Klessig DF (2009) Salicylic Acid, a Multifaceted Hormone to Combat Disease. Annu Rev Phytopathol 47: 177–206**
Pubmed: Author and Title
Google Scholar: Author Only Title Only Author and Title

**Wasternack C, Hause B (2013) Jasmonates: Biosynthesis, perception, signal transduction and action in plant stress response, growth and development. An update to the 2007 review in Annals of Botany. Ann Bot 111: 1021–1058**
Pubmed: Author and Title
Google Scholar: Author Only Title Only Author and Title

**Weikl F, Ghirardo A, Schnitzler J-P, Pritsch K (2016) Sesquiterpene emissions from Alternaria alternata and Fusarium oxysporum: Effects of age, nutrient availability and co-cultivation. Sci Rep 6: 22152**
Pubmed: Author and Title
Google Scholar: Author Only Title Only Author and Title

**Wellburn AR (1990) Tansley Review No. 24 Why are atmospheric oxides of nitrogen usually phytotoxic and not alternative fertilizers? New Phytol 115: 395–429**
Pubmed: Author and Title
Google Scholar: Author Only Title Only Author and Title

**Widemann E, Miesch L, Lugan R, Holder E, Heinrich C, Aubert Y, Miesch M, Pinot F, Heitz T (2013) The amidohydrolases IAR3 and ILL6 contribute to jasmonoyl-isoleucine hormone turnover and generate 12-hydroxyjasmonic acid upon wounding in arabidopsis leaves. J Biol Chem 288: 31701–31714**
Pubmed: Author and Title
Google Scholar: Author Only Title Only Author and Title

**Wildermuth MC, Dewdney J, Wu G, Ausubel FM (2001) Isochorismate synthase is required to synthesize salicylic acid for plant defence. Nature 414: 562–565**
Pubmed: Author and Title
Google Scholar: Author Only Title Only Author and Title

**Xu Q, Zhou B, Ma C, Xu X, Xu J, Jiang Y, Liu C, Li G, Herbert SJ, Hao L (2010) Salicylic acid-altering Arabidopsis mutants response to NO 2 Exposure. Bull Environ Contam Toxicol 84: 106–111**
Pubmed: Author and Title
Google Scholar: Author Only Title Only Author and Title

**Yoneyama T, Sasakawa H (1979) Transformation of atmospheric NO2 absorbed in spinach leaves. Plant Cell Physiol 20: 263–266**
Pubmed: Author and Title
Google Scholar: Author Only Title Only Author and Title

**Zeevaart AJ (1976) Some effects of fumigating plants for short periods with NO2. Environ Pollut 11: 97–108**
Pubmed: Author and Title
Google Scholar: Author Only Title Only Author and Title

**Zipfel C, Robatzek S, Navarro L, Oakeley EJ, Jones JDG, Felix G, Boller T (2004) Bacterial disease resistance in Arabidopsis through flagellin perception. Nature 428: 764–767**
Pubmed: Author and Title
Google Scholar: Author Only Title Only Author and Title